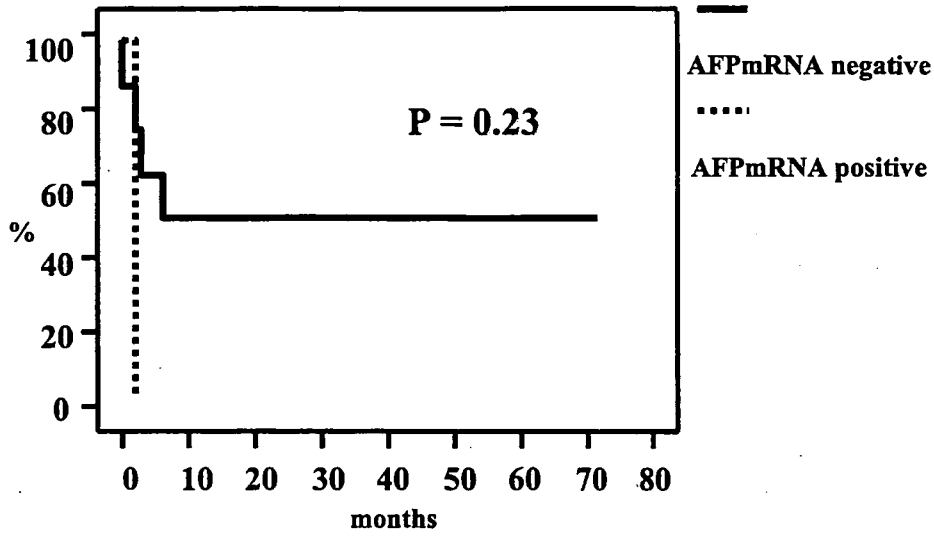

Fig 2. Comparison of recurrence-free survival between AFP mRNA positive and negative patients.

after neoadjuvant immunochemotherapy died 8 months after LDLT due to lung metastases.

These results were evaluated, isolating the effects of the Milan criteria (Fig 1), AFP mRNA expression (Fig 2), and h-TERT mRNA expression (Fig 3) on recurrence-free survival. There was no significant difference between the survival curves without recurrence of patients who did versus did not meet the Milan criteria. There was also no significant difference between the survival curves without recurrence of patients with positive versus negative AFP mRNA expression. However, there was a significant difference (P = .005) between the survival curves without recurrence of patients with positive preoperative h-TERT mRNA expression versus those who either had an initially negative preoperative h-TERT mRNA or who had converted from positive to negative after neoadjuvant immunochemotherapy.

DISCUSSION

HCC tumor recurrence after liver transplantation is due to clinically undetectable, circulating cancer cells. These cells are believed to have escaped from the native, diseased liver and are not recognized due to a lack of detection techniques. With more precise preoperative detection of these errant cells, clinicians would presumably have a more accurate method of predicting prognosis after LDLT for HCC. We chose to study h-TERT mRNA and AFP mRNA as markers for the presence of circulating cancer cells. In this study, all patients with h-TERT mRNA or AFP mRNA present in their peripheral blood preoperatively experienced tumor recurrence after LDLT. Only 1 of 4 patients who developed recurrent HCC after LDLT had AFP mRNA detected preoperatively, whereas all patients with HCC recurrence after LDLT had h-TERT mRNA detected

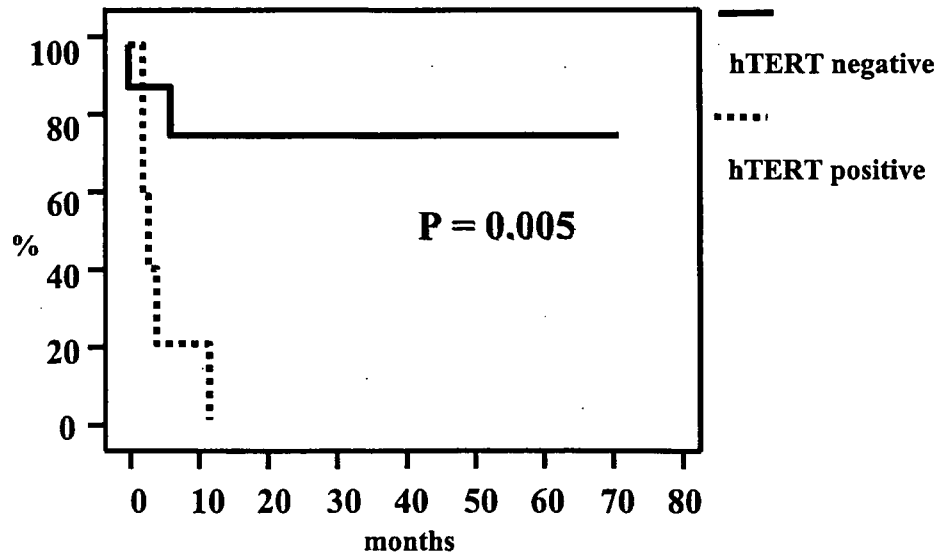

Fig 3. Comparison of recurrence-free survival between h-TERT positive and negative patients.

preoperatively or after neoadjuvant immunochemotherapy. The 2 patients whose h-TERT mRNA expression disappeared after neoadjuvant immunochemotherapy did not develop tumor recurrences, much like the group that had negative h-TERT mRNA expression from the outset. In conclusion, h-TERT mRNA seemed to prove a more valuable number than AFP mRNA, not only for the study of preoperative treatment modalities and postoperative surveillance, but also for evaluation of prospective LDLT patients with HCC. Moreover, h-TERT mRNA could potentially expand the indications for liver transplantation to patients outside the Milan criteria.

REFERENCES

1. Bismuth H, Chiche L, Adam R, et al: Liver resection versus transplantation for hepatocellular carcinoma in cirrhotic patients. Ann Surg 218:145, 1993

2. Yokoyama I, Carr B, Saitsu H, et al: Accelerated growth rates of recurrent hepatocellular carcinoma after liver transplantation. Cancer 68:2095, 1991

3. Sato Y, Ichida T, Suzuki S, et al: Living related donor liver transplantation for preoperative α-fetoprotein mRNA-positive patients of hepatocellular carcinoma: description of five cases. Transplant Proc 35:352, 2003

4. Waguri N, Suda T, Nomoto M, et al: Sensitive and specific detection of circulating cancer cells in patients with hepatocellular carcinoma; detection of human teromerase reverse transcriptase messenger RNA after immunomagnetic separation. Clin Cancer Res 9:3004, 2003

5. Sato Y, Yamamoto S, Oya H, et al: Preoperative human-telomerase reverse transcriptase mRNA in peripheral blood and tumor recurrence in living-related liver transplantation for hepatocellular carcinoma. Hepatogastroenterology 52:1325, 2005

6. Mazzaferro V, Regaria E, Doci R, et al: Liver transplantation for the treatment of small hepatocellular carcinomas in patients with cirrhosis. N Engl J Med 334:693, 1996

7. Sato Y, Ichida T, Ito S, et al: Preoperative administration of 5FU and IFN-β may prevent recurrence of hepatitis B and C virus. Am J Gastroenterol 97:215, 2002

STEM CELLS
TISSUE-SPECIFIC STEM CELLS

Long-Term Culture of Postnatal Mouse Hepatic Stem/Progenitor Cells and Their Relative Developmental Hierarchy

ATSUNORI TSUCHIYA,[a,b] TOSHIO HEIKE,[a] SHIRO BABA,[a] HISANORI FUJINO,[a] KATSUTSUGU UMEDA,[a] YASUNOBU MATSUDA,[b] MINORU NOMOTO,[b] TAKAFUMI ICHIDA,[c] YUTAKA AOYAGI,[b] TATSUTOSHI NAKAHATA[a]

[a]Department of Pediatrics, Graduate School of Medicine, Kyoto University, Kyoto, Japan; [b]Division of Gastroenterology and Hepatology, Graduate School of Medical and Dental Science, Niigata University, Niigata, Japan; [c]Department of Gastroenterology, Juntendo University School of Medicine, Izunokuni, Japan

Key Words. Side population cells • Sca-1+ cells • Serum-free medium • Long-term culture Fluorescence-activated cell sorting analysis • Hepatic stem cells

ABSTRACT

Few studies on the long-term culture of postnatal mouse hepatic stem/progenitor cells have been reported. We successfully adapted a serum-free culture system that we employed previously to expand fetal mouse hepatic stem/progenitor cells and maintained them in culture over long periods. The expanded postnatal cells contained immature α-fetoprotein-positive cells along with hepatocytic and cholangiocytic lineage-committed cells. These cells expressed CD49f but not CD45, CD34, Thy-1, c-kit, CD31, or flk-1, and oncostatin M induced their differentiation. This heterogeneous population contained side population (SP) cells, which express the ATP-binding cassette transporter ABCG2, and sca-1+ cells. As mice aged, the frequency of SP and sca-1+ cells decreased along with the ability of cultured cells to expand. Approximately 20%–40% of the SP cells expressed sca-1, but only a few sca-1+ cells were also SP cells. Analysis of colonies derived from single SP or sca-1+ cells revealed that, although both cells had dual differentiation potential and self-renewal ability, SP cells formed colonies more efficiently and gave rise to SP and sca-1+ cells, whereas sca-1+ cells generated only sca-1+ progeny. Thus, SP cells are more characteristic of stem cells than are sca-1+ cells. In regenerating livers, ABCG2+ cells and sca-1+ cells were detected around or in the portal area (the putative hepatic stem cell niche). The expanded cells share many features of fetal hepatic stem/progenitor cells or oval cells and may be useful in determining the mechanisms whereby hepatic stem cells self-renew and differentiate. STEM CELLS *2007;25:895–902*

Disclosure of potential conflicts of interest is found at the end of this article.

INTRODUCTION

Serial cell transplantation studies [1, 2] have revealed that postnatal livers contain populations that can expand over long periods. It remains unclear, however, where in the liver these hepatic stem cells reside. Moreover, although there is evidence for the existence of extrahepatic stem cells, such as bone marrow cells [3] and peripheral blood cells [4], that can travel to the liver and act as hepatic stem cells, it is unclear whether these cells transdifferentiate or fuse with hepatocytes to exert hepatic stem cell function. In addition, although postnatal hepatic stem/progenitor cells have been characterized by several markers, including CD34 [5, 6], c-kit [7–9], Thy-1 [10], sca-1 [11, 12], and side population (SP) cell attributes [12, 13], the location of each marker in the developmental hierarchy of hepatic stem/progenitor cells is not known. Answers to these questions are needed to devise novel strategies for cell transplantation or effectively induce endogenous hepatic stem/progenitor cells required for rapid recovery from severe liver damage. However, progress is hampered by difficulties in maintaining and expanding postnatal hepatic stem/progenitor cells and, consequently, few studies report long-term culture of postnatal liver cells. For example, in mouse, most reports analyze cells from transgenic or mutant mouse donors, namely Met murine hepatocyte cells [14, 15], which are generated from liver of mice expressing an active truncated form of the human Met receptor or from p53 null-transformed hepatic progenitor cells [16]. Two additional studies have sought to establish long-term cultures of hepatic cells from normal postnatal livers. In one, Azuma et al. [17] were relatively successful in maintaining mouse adult hepatic stem/progenitor cells by initially suspending hepatic cells in hypoxic conditions and then allowing them to form aggregates. In the other study, Block et al. have developed hepatocyte growth medium [18], a serum-free medium allowing normal adult hepatocyte expansion. However, neither of these methods permits extensive expansion of adult mouse hepatic stem/progenitor cells with repeated passage. With regard to the long-term culture of postnatal human liver cells, Parent et al. established HepaRG cell lines [19] with dual differentiation potential from a liver associated with chronic hepatitis C infection. However, cell lines with dual differentiation potential have not been established from normal postnatal human livers. Finally, long-term culture of postnatal liver cells from rats has been successfully achieved, including WB-344 [20], rat liver epithelial cells [21], and hepatic stem-like epithelial cells [22, 23]. However,

Correspondence: Tatsutoshi Nakahata, M.D., Department of Pediatrics, Graduate School of Medicine, Kyoto University, 54 Kawara-cho, Shogoin, Sakyo-ku, Kyoto 606-8507, Japan. Telephone: +81-75-751-3290; Fax: +81-75-752-2361; e-mail: tnakaha@kuhp.kyoto-u.ac.jp
Received September 3, 2006; accepted for publication December 27, 2006; first published online in STEM CELLS *EXPRESS* January 11, 2007.
 1066-5099/2007/$30.00/0 doi: 10.1634/stemcells.2006-0558

markers of all of these cells have not been comprehensively assessed, and thus their place in the stem cell developmental hierarchy remains unknown.

Recently, we established a long-term culture system that permits extensive expansion of normal mouse fetal hepatic stem/progenitor cells [12]. This system employs serum-free medium containing B27, hepatocyte growth factor (HGF), basic fibroblast growth factor (bFGF), and epidermal growth factor (EGF). This system generates large colonies more readily than previously reported systems. The method utilizes a replating procedure employing diluted trypsin with knockout serum replacement and $CaCl_2$, thus maintaining cell-cell contact and viability. The resulting expanded fetal hepatic stem/progenitor cell populations are a heterogeneous mixture of cells including SP (5%–20%) and sca-1+ (approximately 15%) cells. Using these two stem cell markers, we could further enrich the population of fetal hepatic stem/progenitor cells.

In this study, we modified the culture system described above and succeeded in expanding postnatal hepatic stem/progenitor cells from undamaged postnatal livers. These cells could be maintained over the long periods by passage and are a heterogeneous mixture of cells that include SP and sca-1+ cells. Our previous study suggested that these cells have stem cell characteristics [12], and, indeed, we show here that both types proliferate and have bipotential differentiation ability. We also analyzed the place in the hierarchy of stem cell development that these cells occupy by purifying single SP and sca-1+ cells and evaluating their progeny. Finally, we examined the in vivo expression of the SP phenotype or sca-1 in normal and damaged livers.

MATERIALS AND METHODS

Mice

C57BL/6 mice (4-, 8-, 12-week-old; n = 5 per age group) were obtained from SLC (Hamamatsu, Japan, http://www.jslc.co.jp). Liver tissue served as the source of postnatal hepatic stem/progenitor cells. Regenerating livers were induced by injecting 4-week-old C57BL/6 mice intraperitoneally three times at 2-day intervals with anti-mouse Fas (0.3 mg/kg) (BD Pharmingen, San Diego, http://www.bdbiosciences.com/index_us.shtml) [24] dissolved in phosphate-buffered saline (PBS). Five days after the last injection, regenerating livers were removed and analyzed. Mice were maintained according to Animal Protection Guidelines of Kyoto University (Kyoto, Japan).

Hepatic Cell Culture

Hepatic cells were dissociated using a 2-step collagenase method, collected by centrifugation at 500 rpm for 2 minutes, suspended in Dulbecco's modified Eagle's medium/F12 (Sigma-Aldrich, St. Louis, http://www.sigmaaldrich.com) with B27 (Gibco, Grand Island, NY, http://www.invitrogen.com), ITS-X (Gibco), 10 mM HEPES (Nacalai Tesque Inc., Kyoto, Japan, http://www.nacalai.co.jp/en), antibiotics, 20 ng/ml EGF (Sigma-Aldrich), 20 ng/ml bFGF (R&D Systems Inc., Minneapolis, http://www.rndsystems.com), and 10 ng/ml HGF (Peprotech, Rocky Hill, NJ, http://www.peprotech.com), and finally plated onto 6-cm-diameter type 1 collagen-coated dishes (1×10^5 cells per dish). This standard medium was changed every 3 days. On day 14, cells were harvested using diluted trypsin [12] and plated onto newly prepared collagen-coated dishes. On day 21, the colonies that contained more than 200 cells were counted and expanded.

Reverse Transcription-Polymerase Chain Reaction Analysis

Total RNA was prepared by using TRIzol (Invitrogen, Carlsbad, CA, http://www.invitrogen.com) and reverse-transcribed using a SuperScript first-strand synthesis system (Invitrogen). cDNA was amplified by polymerase chain reaction (PCR) with the AmpliTaq Gold kit (Applied BioSystems, Foster City, CA, http://www.appliedbiosystems.com), and PCR was performed with primers specific for transcripts encoding the following proteins: the immature cell marker α-fetoprotein (AFP); hepatocyte-specific markers albumin (ALB), α1-antitrypsin (α1-A), glucose-6 phosphatase (G-6-P) [25], tyrosine amino transferase (TAT) [26], and tryptophan-2,3-dioxygenase (TO); cholangiocyte-specific markers cytokeratin (CK)19 and biliary glycoprotein (BGP) [25]; and internal control β-actin (β-act). The oligonucleotide primers were: AFP: 5′-ACT CAC CCC AAC CTT CCT GTC-3′ 5′-CAG CAG TGG CTG ATA CCA GAG-3′, ALB: 5′-CAT GAC ACC ATG CCT GCT GAT-3′ 5′-CTC TGA TCT TCA GGA AGT GTA-3′, α1-A: 5′-TCG ATC CTA AGC ACA CTG AGG-3′ 5′-CGG CTT GTA AGA CTG TAG C-3′, G-6-P: 5′-AAC CCA TTG TGA GGC CAG AGG-3′ 5′-TAC TCA TTA CAC TAG TTG GTC-3′, TAT: 5′-TCC AGG AGT TCT GTG AAC AGC-3′ 5′-AGT ATA TGG TGC CTG CCT GC-3′, TO: 5′-TGC GCA AGA ACT TCA GAG TGA-3′ 5′-AGC AAC AGC TCA TTG TAG TCT-3′, CK19: 5′-GTC CTA CAG ATT GAC AAT GC-3′ 5′-CAC GCT CTG GAT CTG TGA CAG-3′, BGP: 5′-GAA CTA GAC TCT GTC ACC CTG-3′ 5′-GCC AGA CTT CCT GGA ATA GA-3′, and β-act: 5′-ATC CTG ACC CTG AAG TAC CCC ATT-3′ 5′-CCA AGA AGG AAG GCT GGA AAA GAG-3′. The following conditions were employed for amplification: initial denaturation at 95°C for 9 minutes followed by 28 (ALB, AFP, and CK19), 30 (β-act), or 35 cycles (others) of 94°C for 30 seconds, 56°C for 30 seconds, 72°C for 30 seconds, and a final extension step at 72°C for 10 minutes. PCR products were then separated on 1.0% agarose gels.

Flow Cytometry

For fluorescence-activated cell sorting (FACS), we used the following markers: rat and human oval cell markers CD34 [5, 6], Thy-1 [10], and c-kit [7–9]; the α6 integrin subunit CD49f [25]; the hematopoietic marker CD45 [27]; the vascular endothelium marker CD31 [28]; the early mesodermal marker flk-1 [29]; and the stem/progenitor cell marker sca-1 [11, 12]. We also used FACS to identify SP cells [13], identifiable by their ability to exclude dyes such as Hoechst due to the expression of the transporter proteins ABCG2/BCRP1 [30]. For FACS analysis, cells (6–12 weeks after plating) from 4-week-old mice were harvested with cell recovery solution (Becton, Dickinson and Company, Franklin Lakes, NJ, http://www.bd.com) for 20 minutes. The resulting cells were incubated with anti-mouse CD16/32 antibodies (BD Pharmingen) for 15 minutes on ice to block nonspecific binding and then incubated with fluorescein isothiocyanate (FITC)-conjugated sca-1, CD34, and Thy-1 antibodies, phycoerythrin (PE)-conjugated CD49f, CD31, and flk-1 antibodies, or allophycocyanin (APC)-conjugated c-kit and CD45 antibodies (BD Pharmingen) for 30 minutes on ice. FITC-conjugated rat IgG2a antibodies, PE-conjugated rat IgG2a antibodies, or APC-conjugated rat IgG2b antibodies (BD Pharmingen) were served as isotype controls. Dead cells were excluded by propidium iodide gating. Hoechst staining was performed as described previously [12]. After washing, the cells were analyzed or sorted by using FACSCalibur, BD LSR, or FACSVantage with the CellQuest program (Becton, Dickinson and Company). To analyze the relative developmental hierarchy of putative stem cells, expanded cells derived from 4-week-old mice were fractionated into four subpopulations using FACSVantage: SP sca-1− cells (group 1), SP sca-1+ cells (group 2), main population (MP) sca-1+ cells (group 3), and MP sca-1− cells (group 4). Our usual sorting procedure yielded purities of approximately 90%–95%. Single cells of each fraction were cultured in individual wells of 96-well type 1 collagen-coated dishes and confirmed microscopically. On day 14 after sorting, large colonies occupying more than 30% of the well surface were counted. Finally, five colonies representing SP sca-1− cells (group 1) and MP sca-1+ cells (group 3) were randomly collected and expanded. On day 24 after sorting, the frequency of SP cells and sca-1+ cells was determined and reverse transcription (RT)-PCR was performed with AFP, ALB, and CK19 primers.

Differentiation Culture Condition

To induce the differentiation of hepatocytic lineage cells, cells from 4-week-old mice that had been expanded for more than 6 weeks were employed. Expanded cells (5×10^5 cells per milliliter) were cultured with standard medium plus 10 ng/ml oncostatin M (OSM; R&D Systems) [31, 32]. OSM at that concentration was added every 3 days when the medium was changed. On day 6, RT-PCR, periodic acid-Schiff (PAS) staining, and immunocytochemistry for carbamoyl phosphate synthetase I (CPSI; Santa Cruz Biotechnology, Santa Cruz, CA, http://www.scbt.com) [33] were performed. On day 9, the frequencies of SP cells, and sca-1+ cells were determined using FACSCalibur, BD LSR, and FACSVantage.

Immunochemical Staining

Immunocytochemistry was performed as described previously [12]. The primary antibodies used were: goat anti-mouse ALB (Bethyl Inc., Montgomery, TX, http://www.bethyl.com), rabbit anti-human AFP (ICN Biochemicals, Costa Mesa, CA, http://www.mpbio.com), mouse anti-CK7 (Progen Industries Limited, Queensland, Australia, http://www.progen.com.au), goat anti-CPSI, and rat anti-mouse sca-1 (BD Pharmingen). Secondary antibodies used were FITC-conjugated donkey anti-goat IgG, Cy3-conjugated donkey anti-goat IgG, FITC-conjugated donkey anti-rabbit IgG, Cy3-conjugated donkey anti-rabbit IgG, FITC-conjugated donkey anti-mouse IgG, and Cy3-conjugated donkey anti-rat IgG (Jackson Immunoresearch Laboratories, West Grove, PA, http://www.jacksonimmuno.com). Normal IgG of the species from which primary antibodies had been obtained served as primary antibodies in the negative controls. PAS staining was performed as described [34]. For immunohistochemistry, livers were collected, fixed in 10% formalin, and embedded in paraffin blocks. Sections 4-μm thick were cut and placed on silane-coated slides. After removing paraffin, endogenous peroxidase activity was blocked with 3% hydrogen peroxide in methanol (Wako Chemical, Osaka, Japan, http://www.wako-chem.co.jp/english) for 10 minutes at room temperature, and sections were incubated with primary antibodies diluted with PBS containing 0.1% saponin. Primary antibodies used were rat anti-mouse sca-1, rabbit anti-ABCG2 (Kamiya Biomedical Company, Seattle, WA, http://www.kamiyabiomedical.com), mouse anti-CK19 (DAKO, Glostrup, Denmark, http://www.dako.com), and rabbit anti-cow CK (Z0622; DAKO), which detects bile ducts and oval cells [35]. Slides were then stained by using Histofine Simple Stain Max-PO (Nichirei, Tokyo, http://www.nichirei.co.jp/english/index.html) and DAB Substrate Kit (Vector Laboratories, Burlingame, CA, http://www.vectorlabs.com) for sca-1, Vectastain ABC Kit and DAB Substrate Kit (Vector Laboratories) for anti-ABCG2 and anti-cow CK, and DAB Substrate Kit, M.O.M Kit, and Vectastain ABC Kit (Vector Laboratories) for anti-CK19. Nuclei were stained using Mayer's hematoxylin solution (Wako Chemical).

Statistical Analysis

The data are presented as mean ± SD. Student's t test was used to determine the statistical significance of observed differences.

RESULTS

Effective Expansion of Postnatal Hepatic Stem/Progenitor Cells and Analysis of Their Characteristics

We previously showed that we could extensively expand fetal hepatic stem/progenitor cells using our standard medium [12]. Therefore, we sought to expand postnatal hepatic stem/progenitor cells using the same medium. Hepatic cells originated from 4-, 8-, and 12-week-old male mice (n = 5, in each group). Initially, we directly cultured sorted cells obtained after liver dissociation; however, this procedure led to poor cell viability. Subsequently, we centrifuged a whole cell preparation at 500 rpm for 2 minutes, since our early studies showed that single fetal liver stem/progenitor cells that were expanded with our culture system could be collected by this centrifugation step. The resulting pellet consisted largely of mature hepatocytes, and the supernatant contained nonparenchymal cells. When the supernatant was cultured, the nonparenchymal cells, such as endothelial cells, hematopoietic cells, and stellate cells, showed rapid growth, but extensive expansion of hepatic stem/progenitor cells was not observed (data not shown). By contrast, when 1×10^6 pellet cells were plated on 6-cm type 1 collagen-coated dishes, rapid growth of endothelial cells, hematopoietic cells, and stellate cells was not detected, but rather expansion of hepatic stem/progenitor cells was observed. The plated hepatic cells first attached to dishes as a monolayer, and some formed floating and attaching spheroids that did not grow. By day 14, after repeated medium changes at 3-day intervals, most cells forming monolayer sheets or spheroids had died, leaving small polygonal living cells (Fig. 1A). On day 14, the cells were passaged for the first time using diluted trypsin, which maintains cell-cell contact. Harvested cells were replated on collagen-coated dishes using our standard medium. On day 21, we determined the frequency of the dishes containing large colonies (more than 200 cells) and found that the frequency of the dishes obtained from the 4-, 8-, and 12-week-old mice was 40%, 20%, and 0%, respectively. During subsequent culturing, these large colonies gradually expanded (Fig. 1B, 1C), and by day 45, stable expansion of cells was observed (Fig. 1D). These stable expanding cells formed heterogeneous populations containing immature AFP+ cells, hepatocytic lineage cells (ALB+ cells), and cholangiocytic lineage cells (CK7+ cells) (Fig. 1E, 1F).

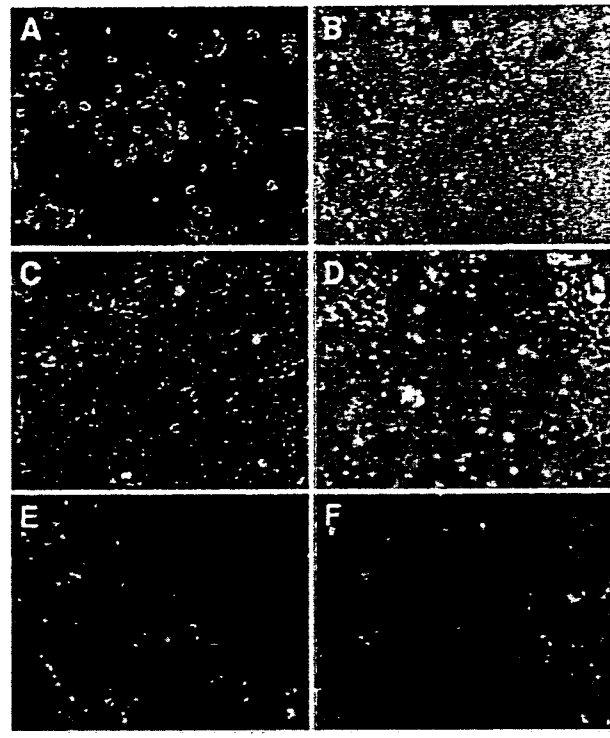

Figure 1. Culture and immunocytochemistry of expanded cells. **(A–D):** Time course of cell culture. These images were obtained from cultured cells from 4-week-old mice. **(A):** Cultures on day 14 just prior to the first passage: some small expanding cells can be seen. **(B, C):** Cultures on day 30: large colonies have formed. **(D):** Cultures on day 45: stably expanding cells can be detected. **(E, F):** Analysis of expanding cells shown in **(D)** with regard to α-fetoprotein (AFP) expression **([E, F]**; red), albumin (ALB) expression **([E]**; green), AFP and ALB expression **([E]**; yellow), and cytokeratin 7 expression **([F]**; green) (original magnification: **[B]**, ×40; **[A, C, E, F]**, ×100; **[D]**, ×200).

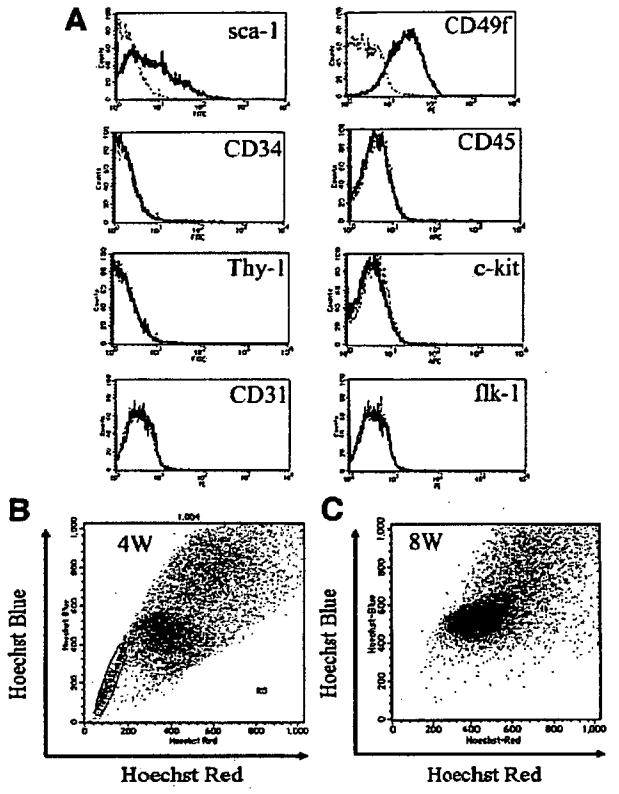

Figure 2. Flow cytometric analysis of expanded cells. **(A):** Flow cytometric analysis of day 45 expanded cells showing that these heterogeneous cells are CD45−, CD34−, Thy-1−, c-kit−, CD31−, flk-1−, and CD49f+~low+. Sca-1+ cells are also detected. **(B, C):** Day 45 expanded cells originating from 4-week-old mice include side population cells **(B)**, unlike cultures derived from 8-week-old mice **(C)**. Abbreviations: 4W, 4-week-old mice; 8W, 8-week-old mice; APC, allophycocyanin; FITC, fluorescein isothiocyanate; PE, phycoerythrin.

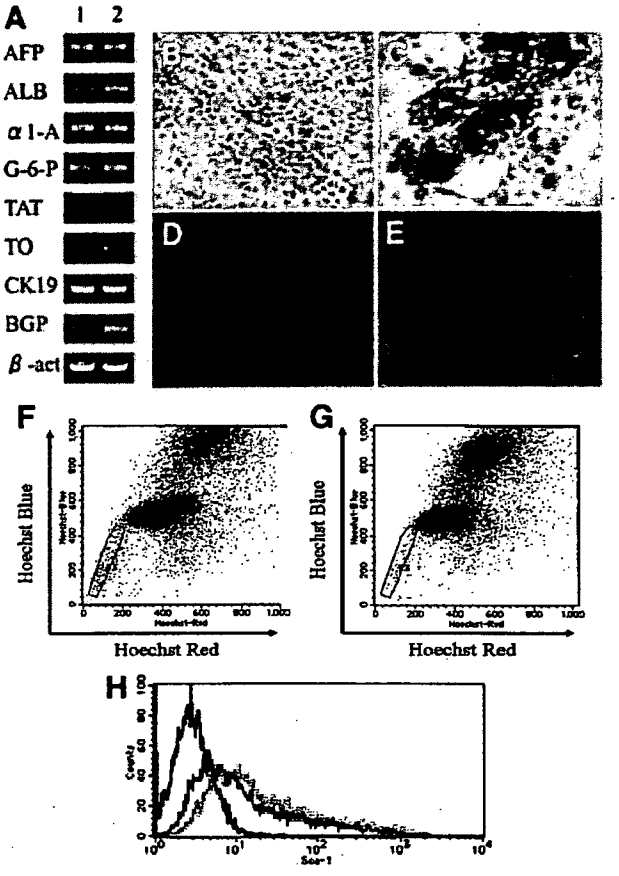

Figure 3. Induction of differentiation by oncostatin M (OSM) treatment. **(A):** Before adding OSM, expanded cells continued to express genes encoding AFP, ALB, α1-A, G-6-P, CK19, and BGP (lane 1). However, on day 6 after addition of OSM, hepatocytic differentiation markers TAT and TO are induced (lane 2). **(B–E):** Compared with untreated cells **(B, D)**, OSM treatment generates cells strongly positive for periodic acid-Schiff **(C)** and carbamoyl phosphate synthetase I **([E]**; red) by day 6. **(F, G):** Flow cytometric analysis indicates that, 9 days after adding OSM, the frequency of side population cells decreases **(F, G)**, whereas that of sca-1+ cells increases **([H]**; black line, isotype control; blue line, sca-1 positivity before adding OSM; red line, sca-1 positivity after adding OSM) (original magnification: **[B–E]**, ×200). Abbreviations: α1-A, α1-antitrypsin; β-act, β-actin; AFP, α-fetoprotein; ALB, albumin; BGP, biliary glycoprotein; CK, cytokeratin; G-6-P, glucose-6 phosphatase; TAT, tyrosine amino transferase; TO, tryptophan-2,3-dioxygenase.

The expanded cultures maintained these phenotypes after further passages. AFP+ cells were relatively smaller than the ALB+ cells and the CK7+ cells (Fig. 1E, 1F). Notably, whereas cells from 4-week-old mice could be maintained for over 30 passages, cells from 8-week-old mice could only be maintained for approximately 20 passages and then gradually lost their ability to expand. Flow cytometric analysis of expanded heterogeneous day 45 cells revealed that they expressed CD49f (+~low) but not CD45, CD34, Thy-1, c-kit, CD31, or flk-1 (Fig. 2A). This was true for both 4- and 8-week-old mouse-derived cultures. SP cells and/or sca-1+ cells were also found in heterogeneous expanded cell populations; however, the frequencies of SP cells and sca-1+ cells in the population varied depending on the age of the donor mouse. Thus, whereas 2%–4% and 15%–40% of the expanded cells from 4-week-old mice were SP and sca-1+, respectively, cell populations from 8-week-old mice showed fewer sca-1+ cells (approximately 1%) and no SP cells (Fig. 2B, 2C). Thus, our culture system can successfully generate long-term postnatal hepatic cell cultures containing cells expressing immature markers.

Differentiation Induced by Oncostatin M

To determine whether expanded cells can differentiate into cells expressing hepatocytic lineage differentiation markers, we employed OSM treatment. Cultured cells from 4-week-old mice that had been expanded for over 6 weeks were differentiated in standard medium containing OSM. RT-PCR, PAS staining, and immunocytochemistry were performed 6 days later and flow cytometric analysis was performed on day 9. Before cells were treated with OSM, they expressed genes encoding AFP, ALB, α1-A, G-6-P, CK19, and BGP but did not express the hepatocytic differentiation markers TAT and TO (Fig. 3A). However, RT-PCR analysis revealed that TAT and TO mRNAs were induced by day 6 after OSM treatment (Fig. 3A). PAS staining and immunocytochemistry for CPSI also revealed relatively large PAS-positive (Fig. 3B, 3C) and CPSI-positive (Fig. 3D, 3E) cells on day 6. Thus, expanded cells can differentiate into mature hepatocytes. Flow cytometric analysis on day 9 revealed that OSM treatment reduced the growth rate by approximately 85% compared with untreated controls (data not shown). Interestingly, although 9 days of OSM treatment reduced the frequency of SP cells by approximately 45% (Fig. 3F, 3G), it increased the frequency of sca-1+ cells by approximately 50% compared with the untreated controls (Fig. 3H).

SP Cells Are More Likely to Be Stem Cells Than Are Sca-1+ Cells

Next, we asked whether SP cells and/or sca-1+ cells in our culture have stem cell characteristics and whether one of these two cell populations is derived from the other. Initially, we compared the size of these cells and the frequency of cells that showed both the SP attribute and expressed sca-1. Flow cytometric analysis revealed that SP cells were relatively smaller than sca-1+ cells (Fig. 4A, 4B, 4D, 4E). Moreover, 20%–40% of the SP cells were also sca-1+, whereas less than 5% of the sca-1+ cells were SP cells (Fig. 4A, 4C, 4D, 4F). Immunocytochemical analysis revealed that, although sca-1+ cells were rarely also AFP+ and ALB+ cells, more than 20% of sca-1+ cells were also CK7+ (Fig. 4G–4I).

Next, to determine whether sca-1+ cells are derived from SP cells or vice versa, expanded cells were fractionated into four groups, namely SP sca-1− (group 1), SP sca-1+ (group 2), MP sca-1+ (group 3), and MP sca-1− (group 4), and subjected to single cell culture analysis. Fourteen days after sorting, large colonies occupying more than 30% of the well surface were counted. The frequencies of large colonies per 300 fractionated cells were 42.6 ± 10.5 (group 1), 37.6 ± 2.3 (group 2), 20.3 ± 8.6 (group 3), and 8.6 ± 1.2 (group 4) (Fig. 4J). Thus, SP cells formed colonies more readily than did sca-1+ cells. To analyze further the relationship between SP and sca-1+ cells, five large colonies from group 1 (SP sca-1−) and group 3 (MP sca-1+) were randomly picked and cultured. On day 24, after being sorted, cells were subjected to flow cytometry to determine the frequencies of SP and sca-1+ cells and analyzed for expression of AFP, ALB, and CK19. Flow cytometric analysis revealed that, whereas the SP sca-1− cells gave rise to both SP cells and sca-1+ cells, MP sca-1+ cells produced mainly sca-1+ cells and rarely produced SP cells (Fig. 4K). RT-PCR also revealed that, whereas the progeny of either SP sca-1− or MP sca-1+ cells expressed genes encoding ALB and CK19, cells derived from SP sca-1− cells expressed higher levels of AFP than those derived from MP sca-1+ cells (Fig. 4K). These results indicate that, although SP cells and sca-1+ cells both have self-renewal ability and dual differentiation potential, SP cells are more immature than sca-1+ cells and give rise to sca-1+ cells.

SP Cells and Sca-1+ Cells Reside in the Periportal Area of Regenerating Livers

We next determined whether cells expressing SP and sca-1 stem cell markers are found in normal or regenerating livers by searching for ABCG2-expressing and sca-1-expressing cells. SP phenotype (the ability to exclude dyes) arises from the expression of the ATP-binding cassette transporter ABCG2/BCRP1 [36], and thus SP cells in the liver were identified on the basis of their ABCG2 expression. To induce immature hepatic cells, 4-week-old mice were injected three times at 2-day intervals with anti-mouse Fas (0.3 mg/kg) dissolved in PBS. Five days after the last injection, regenerating livers were removed and analyzed. Many ductular proliferating cells that were positive for anti-cow CK and exhibiting oval cell morphology were apparent (Fig. 5A–5D). The luminal surface of the ductular proliferating cells in the portal area strongly expressed ABCG2 (Fig. 5F). By contrast, in normal liver, only the canalicular membrane of hepatocytes weakly expressed ABCG2 (Fig. 5E). With regard to sca-1, sca-1 positivity in liver was not restricted to hepatic stem/progenitor cells but was also seen in endothelial cells, hematopoietic cells, and other cells including hepatic stem/progenitor cells (data not shown). Endothelial cells around the portal area in the regenerating liver strongly expressed sca-1 (Fig. 5H), whereas the same cells in the normal liver showed much weaker expression (Fig. 5G). In the regenerating liver,

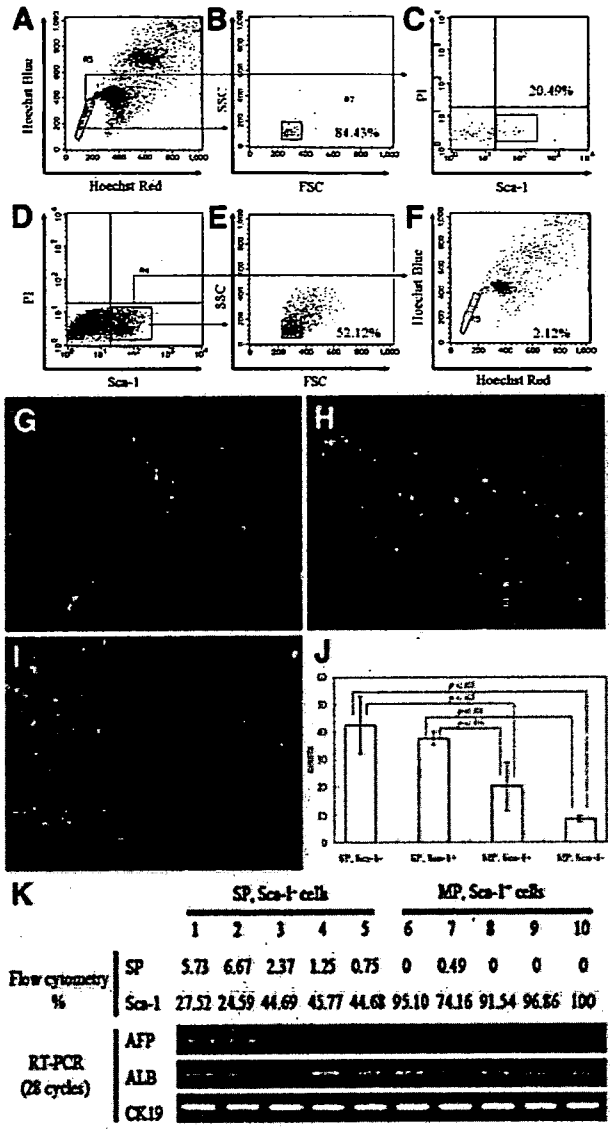

Figure 4. Flow cytometry, immunocytochemistry, and RT-PCR of SP and sca-1+ cells in the expanded populations derived from 4-week-old mice. **(A–F):** SP cells **(A, B)** are smaller than sca-1+ cells **(D, E)**, and 20%–40% of SP cells are sca-1+ **(A, C)**, whereas less than 5% of sca-1+ cells exhibit the SP phenotype **(D, F)**. Immunocytochemistry shows that, whereas sca-1+ cells ([G–I]; red) rarely express AFP ([G]; green) or ALB ([H]; green), more than 20% of sca-1+ cells express CK7 ([I]; green). **(J):** The expanded cell population was fractionated into indicated subpopulations, which were then cultured at the single-cell level. Numbers of large colonies arising from fractionated cells by day 14 after sorting and plating were determined. This revealed that SP cells have an enhanced ability to form colonies, unlike sca-1+ cells. **(K):** Single cell culture of SP and sca-1+ cells. We randomly collected 1–5 large colonies from single SP sca-1− cells and 6–10 from single MP sca-1+ cells. Flow cytometric analysis revealed that, whereas the SP sca-1− cells give rise to both SP cells and sca-1+ cells, MP sca-1+ cells produce mainly sca-1+ cells. RT-PCR also reveals that, whereas both SP sca-1− and MP sca-1+ cells have bipotential differentiation potential, cells derived from SP sca-1− cells express higher levels of AFP than those derived from MP sca-1+ cells (original magnification: [G–I], ×100). Abbreviations: AFP, α-fetoprotein; ALB, albumin; CK, cytokeratin; FSC, forward scatter; MP, main population; PI, propidium iodide; RT-PCR, reverse transcription-polymerase chain reaction; SP, side population; SSC, side scatter.

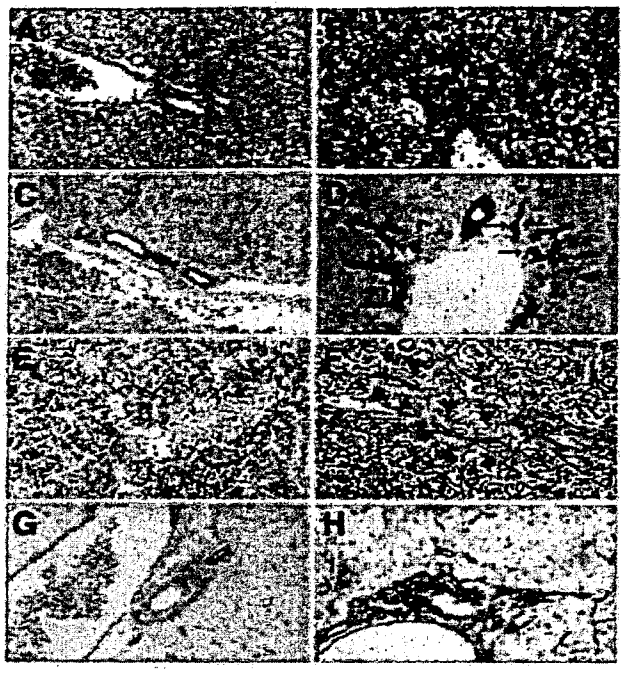

Figure 5. Immunohistochemical analysis of cytokeratin (CK)19, ABCG2, and sca-1 expression in normal and regenerating livers. **(A, B):** Histological analysis of normal liver **(A)** and regenerating liver damaged by anti-mouse Fas **(B)**. Many ductular proliferating cells resembling oval cells are detected in damaged but not normal livers **(B)**. **(C, D):** Immunohistochemical analysis of damaged liver indicates CK19+ bile duct cells **(C)** and ductular proliferating cells positive for anti-cow CK, which detects bile ducts and oval cells **([D]**; arrows). **(E, F):** Immunohistochemical analysis of ABCG2 expression in normal **(E)** and damaged **(F)** livers. Hepatocytes in normal liver express ABCG2 **(E)**, whereas the luminal surface of the ductular proliferating cells in regenerating liver expresses ABCG2 strongly **([F]**; arrowheads). **(G, H):** Immunohistochemical analysis of sca-1 expression in normal **(G)** and regenerating **(H)** liver. In normal liver, sca-1+ endothelial cells surrounding the portal area are detected, whereas in regenerating livers, this expression was stronger, and some bile duct cells also express sca-1 (original magnification: **[A–D, G, H]**, ×200; **[E, F]**, ×400).

although sca-1-expressing cells were mainly endothelial cells, some terminal bile duct cells and interlobular bile duct cells also expressed sca-1 (Fig. 5H). Ductular proliferating cells expressing ABCG2 rarely expressed sca-1 (data not shown). These observations indicate that the portal area is a likely hepatic stem cells niche.

DISCUSSION

Our Culture System Enables Expansion of Postnatal Hepatic Stem/Progenitor Cells In Vitro

To date, many reports describe expansion of fetal hepatic stem/progenitor cells [25, 37–39] but few address expansion of postnatal hepatic stem/progenitor cells. Moreover, long-term expansion with passage of normal postnatal mouse hepatic stem/progenitor cells has not been achieved. In addition, phenotype of postnatal hepatic stem/progenitor cells and how these cells are related developmentally to other stem cells have not been thoroughly analyzed. Recently, we established a culture system that permits the extensive expansion of mouse fetal hepatic stem/progenitor cells. This culture system allows large colonies to be subcultured in a way that maintains cell-cell contact. Subculturing of postnatal hepatic stem/progenitor cells is a major impediment to their long-term expansion. Here, when we used our culture system with postnatal hepatic stem/progenitor cells, we could expand and maintain them over multiple passages. Notably, whereas fetal hepatic stem/progenitor cells easily form expanding spheroids, which then form large monolayer colonies after being plated on collagen, postnatal hepatic cells did not form expanding spheroids and generated monolayer colonies at an extremely low rate (Table 1). Such rare large colonies became increasingly rarer as the age of donor mice increased (Table 1). Nevertheless, our ability to expand postnatal hepatic cells with this culture system indicates that the postnatal liver contains cells with extensive growth ability.

Table 1. Comparison of expanded cells derived from postnatal livers with those derived from fetal livers

Mice	SP cells (%)	Sca-1+ cells (%)	Dishes containing large colonies (%)
E13.5 day	>5	~15	100
4-Week-old	2–4	~15–40	40
8-Week-old	<1	~1	20

Abbreviation: SP, side population.

Expanded Cells Contain SP and Sca-1+ Cells in a Developmental Hierarchy

The expanded postnatal liver cells were heterogeneous populations containing immature AFP+ cells, hepatocytic lineage cells, and cholangiocytic lineage cells. Flow cytometric analysis of these heterogeneous cells revealed that they expressed CD49f (+~low+) but not CD45, CD34, Thy-1, c-kit, CD31, or flk-1. Such marker expression indicates that this cell population is similar to previously reported hepatic stem cells [40] and likely shares similar differentiation potential. Moreover, postnatal expanded cells also contained SP cells and sca-1+ cells, enabling us to assess whether one population gave rise to the other. To do this, we analyzed the expanded population with flow cytometry using the SP and sca-1 markers. That analysis revealed that 2%–4% and 15%–40% of the expanded cells (from 4-week-old mice) were SP+ and sca-1+, respectively, and that 20%–40% of SP cells were sca-1+, whereas less than 5% of the sca-1+ cells were SP cells. When we then expanded individual SP and sca-1+ cells and analyzed the resulting colonies, we found that SP cells formed colonies more efficiently than did sca-1+ cells, and SP cells produced both SP cells and sca-1+ cells, whereas sca-1+ cells almost exclusively generated sca-1+ cells. Moreover, RT-PCR analysis revealed that colonies originating from single SP cells expressed AFP transcripts gene (immature cell marker) at higher levels than did colonies derived from single sca-1+ cells. Finally, flow cytometric analysis showed that OSM treatment decreased the frequency of SP cells, although the frequency of sca-1+ cells increased. These observations together suggest that SP cells are more immature than sca-1+ cells and give rise to the latter. However, since RT-PCR analysis revealed that the colonies derived from single SP and sca-1+ cells all express ALB and CK19 transcripts, it is likely that, like SP cells, sca-1+ cells still have self-renewal ability and dual differentiation potential. All of these observations are similar to those made in the analysis of expanded stem/progenitor cells derived from the fetal liver [12].

Hepatic Stem Cells with Highly Regenerative Potential Decrease with Age

In comparing the number of SP and sca-1+ cells, we found that there were fewer SP cells in the expanded postnatal hepatic

stem/progenitor cell population (2%–4%) than in expanded fetal hepatic stem/progenitor cell populations (more than 5%). This observation suggests that the number of stem cells decreases with age. This idea is supported by observations that (a) SP cells could be expanded from livers of 4-week-old but not 8- or 12-week-old mice, (b) the expanded population from the livers of 8-week-old mice contained fewer sca-1+ cells (approximately 1%) than the 4-week-old liver derived population (15%–40%), and (c) although cells originating from 4-week-old mice could be maintained for over 30 passages, cells from 8-week-old mice could only be maintained for about 20 passages and gradually lost their ability to expand. Thus, we estimate that the number of stem cells with the greatest regenerative ability decreases with age as does liver regenerative potential.

The Periportal Area Is the Niche of Hepatic Stem/Progenitor Cells

We next analyzed which cells in the normal or regenerative livers of 4-week-old mice express the SP cell marker ABCG2 and which express sca-1. In the normal liver, some mature hepatocytes express ABCG2, although the main expression of sca-1 was by the endothelial cells around the portal area. In contrast, in regenerating livers, ductular proliferating cells expressed ABCG2 and some bile duct cells expressed sca-1. These results reveal that ABCG2+ and sca-1+ cells exist in the portal area (the putative hepatic stem cell niche). However, the distribution of ABCG2+ and sca-1+ cells differed. In particular, ABCG2+ cells were found in the vicinity of the canal of Hering, supporting a previous report suggesting that hepatic stem cells are located near this location. Notably, our immunocytochemical analysis revealed that sca-1+ cells also tended to express CK7+ more often than AFP and ALB, suggesting that sca-1+ cells are more likely to be of the cholangiocytic than the hepatocytic lineage.

Utility of Our Expanded Cell System

Our expanded cell populations may be useful in analysis of self-renewal and differentiation of hepatic stem cells. Recent studies showed that, although embryonic stem cells [41, 42] are attractive hepatic stem cell sources for such study, this cell source is problematic because it is difficult to differentiate highly enriched populations of hepatic cells. By contrast, our culture system expands only hepatic cells, making it ideal for characterizing various hepatic stem/progenitor cells in the liver and for assessing their relative position in a developmental hierarchy.

ACKNOWLEDGMENTS

This work was supported by a Grant-in-Aid for Creative Scientific Research (13GS0009) and a Grant-in-Aid for Scientific Research (B) (15039219) from the Ministry of Education, Science, Technology, Sports and Culture of Japan.

DISCLOSURE OF POTENTIAL CONFLICTS OF INTEREST

The authors indicate no potential conflicts of interest.

REFERENCES

1 Rajvanshi P, Kerr A, Bhargava KK et al. Efficacy and safety of repeated hepatocyte transplantation for significant liver repopulation in rodents. Gastroenterology 1996;111:1092–1102.
2 Overturf K, al-Dhalimy M, Ou CN et al. Serial transplantation reveals the stem-cell-like regenerative potential of adult mouse hepatocytes. Am J Pathol 1997;151:1273–1280.
3 Lagasse E, Connors H, Al-Dhalimy M et al. Purified hematopoietic stem cells can differentiate into hepatocytes in vivo. Nat Med 2000;6:1229–1234.
4 Ruhnke M, Ungefroren H, Nussler A et al. Differentiation of in vitro-modified human peripheral blood monocytes into hepatocyte-like and pancreatic islet-like cells. Gastroenterology 2005;128:1774–1786.
5 Omori N, Omori M, Evarts RP et al. Partial cloning of rat CD34 cDNA and expression during stem cell-dependent liver regeneration in the adult rat. Hepatology 1997;26:720–727.
6 Crosby HA, Kelly DA, Strain AJ. Human hepatic stem-like cells isolated using c-kit or CD34 can differentiate into biliary epithelium. Gastroenterology 2001;120:534–544.
7 Matsusaka S, Tsujimura T, Toyosaka A et al. Role of c-kit receptor tyrosine kinase in development of oval cells in the rat 2-acetylaminofluorene/partial hepatectomy model. Hepatology 1999;29:670–676.
8 Fujio K, Evarts RP, Hu Z et al. Expression of stem cell factor and its receptor, c-kit, during liver regeneration from putative stem cells in adult rat. Lab Invest 1994;70:511–516.
9 Blakolmer K, Jaskiewicz K, Dunsford HA et al. Hematopoietic stem cell markers are expressed by ductal plate and bile duct cells in developing human liver. Hepatology 1995;21:1510–1516.
10 Petersen BE, Goff JP, Greenberger JS et al. Hepatic oval cells express the hematopoietic stem cell marker Thy-1 in the rat. Hepatology 1998;27:433–445.
11 Petersen BE, Grossbard B, Hatch H et al. Mouse A6-positive hepatic oval cells also express several hematopoietic stem cell markers. Hepatology 2003;37:632–640.
12 Tsuchiya A, Heike T, Fujino H et al. Long-term extensive expansion of mouse hepatic stem/progenitor cells in a novel serum-free culture system. Gastroenterology 2005;128:2089–2104.
13 Shimano K, Satake M, Okaya A et al. Hepatic oval cells have the side population phenotype defined by expression of ATP-binding cassette transporter ABCG2/BCRP1. Am J Pathol 2003;163:3–9.
14 Bordoni V, Alonzi T, Agrati C et al. Murine hepatocyte cell lines promote expansion and differentiation of NK cells from stem cell precursors. Hepatology 2004;39:1508–1516.
15 Spagnoli FM, Amicone L, Tripodi M et al. Identification of a bipotential precursor cell in hepatic cell lines derived from transgenic mice expressing cyto-Met in the liver. J Cell Biol 1998;143:1101–1112.
16 Dumble ML, Croager EJ, Yeoh GC et al. Generation and characterization of p53 null transformed hepatic progenitor cells: Oval cells give rise to hepatocellular carcinoma. Carcinogenesis 2002;23:435–445.
17 Azuma H, Hirose T, Fujii H et al. Enrichment of hepatic progenitor cells from adult mouse liver. Hepatology 2003;37:1385–1394.
18 Block GD, Locker J, Bowen WC et al. Population expansion, clonal growth, and specific differentiation patterns in primary cultures of hepatocytes induced by HGF/SF, EGF and TGF alpha in a chemically defined (HGM) medium. J Cell Biol 1996;132:1133–1149.
19 Parent R, Marion MJ, Furio L et al. Origin and characterization of a human bipotent liver progenitor cell line. Gastroenterology 2004;126:1147–1156.
20 Tsao MS, Smith JD, Nelson KG et al. A diploid epithelial cell line from normal adult rat liver with phenotypic properties of 'oval' cells. Exp Cell Res 1984;154:38–52.
21 Sanchez A, Factor VM, Espinoza LA et al. In vitro differentiation of rat liver derived stem cells results in sensitization to TNFalpha-mediated apoptosis. Hepatology 2004;40:590–599.
22 Nagai H, Terada K, Watanabe G et al. Differentiation of liver epithelial (stem-like) cells into hepatocytes induced by coculture with hepatic stellate cells. Biochem Biophys Res Commun 2002;293:1420–1425.
23 Oh BK, Lee CH, Park C et al. Telomerase regulation and progressive telomere shortening of rat hepatic stem-like epithelial cells during in vitro aging. Exp Cell Res 2004;298:445–454.
24 Eichhorst ST, Krueger A, Muerkoster S et al. Suramin inhibits death receptor-induced apoptosis in vitro and fulminant apoptotic liver damage in mice. Nat Med 2004;10:602–609.
25 Suzuki A, Zheng Y, Kondo R et al. Flow-cytometric separation and enrichment of hepatic progenitor cells in the developing mouse liver. Hepatology 2000;32:1230–1239.
26 Hoppo T, Fujii H, Hirose T et al. Thy1-positive mesenchymal cells promote the maturation of CD49f-positive hepatic progenitor cells in the mouse fetal liver. Hepatology 2004;39:1362–1370.
27 Umeda K, Heike T, Yoshimoto M et al. Development of primitive and definitive hematopoiesis from nonhuman primate embryonic stem cells in vitro. Development 2004;131:1869–1879.

28 Medina J, Arroyo AG, Sanchez-Madrid F et al. Angiogenesis in chronic inflammatory liver disease. Hepatology 2004;39:1185–1195.
29 Iida M, Heike T, Yoshimoto M et al. Identification of cardiac stem cells with FLK1, CD31, and VE-cadherin expression during embryonic stem cell differentiation. Faseb J 2005;19:371–378.
30 Alison MR. Tissue-based stem cells: ABC transporter proteins take centre stage. J Pathol 2003;200:547–550.
31 Kamiya A, Kinoshita T, Ito Y et al. Fetal liver development requires a paracrine action of oncostatin M through the gp130 signal transducer. Embo J 1999;18:2127–2136.
32 Miyajima A, Kinoshita T, Tanaka M et al. Role of Oncostatin M in hematopoiesis and liver development. Cytokine Growth Factor Rev 2000;11:177–183.
33 Strick-Marchand H, Morosan S, Charneau P et al. Bipotential mouse embryonic liver stem cell lines contribute to liver regeneration and differentiate as bile ducts and hepatocytes. Proc Natl Acad Sci U S A 2004;101:8360–8365.
34 Minguet S, Cortegano I, Gonzalo P et al. A population of c-Kit-(low)(CD45/TER119)- hepatic cell progenitors of 11-day postcoitus mouse embryo liver reconstitutes cell-depleted liver organoids. J Clin Invest 2003;112:1152–1163.
35 Kofman AV, Morgan G, Kirschenbaum A et al. Dose- and time-dependent oval cell reaction in acetaminophen-induced murine liver injury. Hepatology 2005;41:1252–1261.
36 Zhou S, Schuetz JD, Bunting KD et al. The ABC transporter Bcrp1/ABCG2 is expressed in a wide variety of stem cells and is a molecular determinant of the side-population phenotype. Nat Med 2001;7:1028–1034.
37 Malhi H, Irani AN, Gagandeep S et al. Isolation of human progenitor liver epithelial cells with extensive replication capacity and differentiation into mature hepatocytes. J Cell Sci 2002;115:2679–2688.
38 Strick-Marchand H, Weiss MC. Inducible differentiation and morphogenesis of bipotential liver cell lines from wild-type mouse embryos. Hepatology 2002;36:794–804.
39 Lazaro CA, Croager EJ, Mitchell C et al. Establishment, characterization, and long-term maintenance of cultures of human fetal hepatocytes. Hepatology 2003;38:1095–1106.
40 Kamiya A, Gonzalez FJ, Nakauchi H. Identification and differentiation of hepatic stem cells during liver development. Front Biosci 2006;11:1302–1310.
41 Teratani T, Yamamoto H, Aoyagi K et al. Direct hepatic fate specification from mouse embryonic stem cells. Hepatology 2005;41:836–846.
42 Yamamoto H, Quinn G, Asari A et al. Differentiation of embryonic stem cells into hepatocytes: Biological functions and therapeutic application. Hepatology 2003;37:983–993.

Available online at www.sciencedirect.com
ScienceDirect
Biochemical and Biophysical Research Communications 354 (2007) 209–215
BBRC
www.elsevier.com/locate/ybbrc

Mtf-1 lymphoma-susceptibility locus affects retention of large thymocytes with high ROS levels in mice after γ-irradiation

Masaki Maruyama [a,b], Takashi Yamamoto [a], Yuki Kohara [a], Yoshinori Katsuragi [a], Yukio Mishima [a,c], Yutaka Aoyagi [b], Ryo Kominami [a,c,*]

[a] *Department of Molecular Genetics, Niigata University Graduate School of Medical and Dental Sciences, Asahimachi 1-757, Niigata 951-8510, Japan*
[b] *Third Department of Internal Medicine, Niigata University School of Medicine, Asahimachi 1-757, Niigata 951-8510, Japan*
[c] *Transdisciplinary Research, Niigata University, Asahimachi 1-757, Niigata 951-8510, Japan*

Received 13 December 2006
Available online 2 January 2007

Abstract

Mouse strains exhibit different susceptibilities to γ-ray-induced thymic lymphomas. Our previous study identified *Mtf-1* (metal responsive transcription factor-1) as a candidate susceptibility gene, which is involved in the radiation-induced signaling pathway that regulates the cellular reactive oxygen species (ROS). To reveal the mechanism for the increased susceptibility conferred by *Mtf-1* locus, we examined early effects of γ-ray on ROS levels *in vivo* and its difference between *Mtf-1* susceptible and resistant congenic mice. Here, we show the detection of clonally growing thymocytes at 4 weeks after irradiation, indicating the start of clonal expansion at a very early stage. We also show that large thymocytes with higher ROS levels and a proliferation capacity were more numerous in the *Mtf-1* susceptible mice than the resistant mice when examined at 7 days after irradiation, although such tendency was not found in mice lacking one allele of *Bcl11b* tumor suppressor gene. This high retention of the large thymocytes, at a high risk for ROS-induced mutation, is a compensatory proliferation and regeneration response to depletion of the thymocytes after irradiation and the response is likely to augment the development of prelymphoma cells leading to thymic lymphomas.

Keywords: Lymphoma susceptibility; Clonal proliferation; ROS; γ-Irradiation; *Mtf-1*

Fractionated whole-body γ-irradiation (4 × 1.75 Gy at weekly intervals) to mice renders the thymus atrophic by inducing thymocyte apoptosis, and atrophic thymuses develop thymic lymphomas, though the incidence varies among mouse strains [1–3]. Prevention of the lymphoma development was demonstrated by transfer of unirradiated bone marrow cells to irradiated mice, which was presumed to supplement intrathymic pre-T cells [4], within 1 week after the last irradiation but not 1 month or later [5,6]. On the other hand, impaired thymocytes at 2 weeks after irradiation, when transferred to thymus of unirradiated mice, were able to develop into lymphomas [7]. These data suggest the generation of 'prelymphoma' cells in the atrophic thymus at a very early stage.

BALB/c and C57BL/6(B6) mouse strains are highly susceptible to radiogenic thymic lymphomas whereas MSM and C3H strains are resistant [8–10]. Our previous genetic study using BALB/c and MSM strains identified *Mtf-1* (metal responsive transcription factor-1) [11,12] as a candidate susceptibility gene to γ-ray-induced thymic lymphomas [13]. The two different *Mtf-1* alleles, BALB/c encoding the serine-type MTF-1 and MSM encoding the proline-type, exhibited distinct transcriptional activation and responses to ionizing radiation (IR).

Exposure of cells to IR leads to production of reactive oxygen species (ROS) in irradiated cells and their progeny which are thought to be the main cause for the delayed genomic instability [14–16]. In response to physiological

* Corresponding author. Fax: +81 25 227 0757.
E-mail address: rykomina@med.niigata-u.ac.jp (R. Kominami).

0006-291X/$ - see front matter © 2006 Elsevier Inc. All rights reserved.
doi:10.1016/j.bbrc.2006.12.192

growth stimulation, the level of ROS also increases and the increase is sufficient for significantly damaging DNA [17–19]. The elevation of ROS activates p53 signaling pathway which in turn controls the ROS level, proliferation, and apoptosis [20,21]. MTF-1, activated by heavy metals such as zinc, is also included in the radiation-induced signaling pathway that responds to and regulates the cellular ROS level [22]. We reasoned that ROS in thymocytes after IR may differ in amount between congenic mice of the different *Mtf-1* genotype. Since ROS is a well-known mutagen contributing generation of more advanced precancerous cells, the number of prelymphoma cells generated may differ between them. In this paper, we examine clonal growth and the ROS levels in thymocytes between susceptible and resistant congenic lines after IR.

Materials and methods

Mice and irradiation. The congenic mouse strain (line-5) of BALB/c background used in this study carried an MSM-derived chromosomal region spanning an approximately 4 Mb interval between *Nds2* and *D4Mit336* on chromosome 4. The mice were obtained by mating of the previously used congenic strain (line-3) [13] with BALB/c after genotyping with nine microsatellite markers within this region. BALB/c mice were purchased from CLEA Japan Inc. (Tokyo, Japan). Mice used in this study were maintained under specific pathogen-free conditions in the animal colony of the Niigata University. Genotyping was carried out with PCR as described previously [13]. Mice were given a whole-body dose of 3 Gy at a dose rate of 1 Gy/min from a broad-beam cesium-137 source when they were at age of 8 weeks. The Ethics Committee for Animal Experimentation of Niigata University approved all experimental procedures involving the mice.

Flow-cytometric analysis and cell sorting. Progeny obtained by mating between the heterozygous congenic mice were irradiated and thymus was isolated at 3, 5, 7, and 14 days after irradiation. Flow-cytometric analysis was performed as previously described [23,24]. In brief, single cell suspensions of thymocytes were prepared from thymus and, $1–2 \times 10^6$ cells were incubated with monoclonal antibodies (mAbs) in phosphate-buffered saline containing 2% fetal calf serum and 0.2% NaN_3 for 20 min at 4 °C. The following monoclonal antibodies were purchased from eBioscience: anti-CD4-FITC or -APC (RM4-5) and anti-CD8-APC (53-6.7). To prevent nonspecific binding of mAbs, we added CD16/32 (93; eBioscience) before staining with labeled mAbs. Dead cells and debris were excluded from the analysis by appropriate gating of FSC and SSC.

ROS levels were determined by incubating the thymocytes with 10 μg/ml dichlorodihydrofluorescein diacetate (DCFH-DA, Molecular Probes, Eugene, OR) for 15 min at 37 °C in the dark. Cells were then placed on ice and kept in the dark until analysis, which was carried out within 30 min. The percent of dead cells was determined by the uptake of propidium iodide (PI) (10 μg/ml) and excluded from analysis. A minimum of 10,000 cells for each sample were analyzed by a FACScan (Becton–Dickinson) flow cytometer. Data were analyzed using the Flow-Jo software (Tree-Star, Inc.).

For BrdU incorporation experiments, we injected mice at 5 days after γ-irradiation at 1.5 Gy intraperitoneally with 100 μl of BrdU solution (10 mg/ml) and thymus was isolated 1 h after. Thymocytes were prepared from the thymus and analyzed with the use of the BD Pharmingen BrdU Flow Kit according to manufacturer's instruction. In brief, cells were suspended at a concentration of $1–2 \times 10^6$ cells/ml, fixed, permeabilized, and incubated with a murine anti-BrdU antibody for 60 min on ice. After washing, cells were incubated with FITC-conjugated goat anti-mouse antibodies for 30 min on ice, washed, and resuspended in PBS containing 20 μl of the 7AAD solution. Cells were resuspended in staining buffer and analyzed by FACScan. As for separation of large and small thymocytes, sorting was carried out on a FACSAria (BD Biosciences).

Nested PCR assay and estimation of deletion frequency. Genomic DNA was isolated from the thymus of mice at 28 days after irradiation. The nested PCR assay for *Bcl11b/Rit1* internal deletions was performed as described previously [25]. First PCR was done with outer primers F1 and R1 for 30 cycles, and the second PCR was done for another 30 cycles with inner primers F1-2 and R1-2. Reaction mixtures were then analyzed by electrophoresis on agarose gels. Sequence analysis was performed to confirm that DNA in the band consisted of *Bcl11b/Rit1* recombinant molecules.

Western blotting. The large and small thymocytes were separated by flow cytometry and analyzed as described previously [23]. Anti-p53 (#9282) was purchased from Cell Signaling Technology.

Results

Clonally growing thymocytes in mice after irradiation

Fig. 1A shows the number of thymocytes in BALB/c mice at various days after irradiation. The number on average at 5 days after was less than 10% of that in unirradiated mice, and then increased greatly in approximately a half of thymuses at 7 days after. The numbers at 10 and 28 days post-irradiation were similar but generally less than those in unirradiated mice. The proliferation of thymocytes seen from 5 to 10 days after is probably a compensatory reaction of thymocytes to depletion of the cells after irradiation.

Our previous study showed that there are a considerable number (10^3–10^4) of thymocytes in unirradiated thymus with intragenic deletions of *Bcl11b/Rit1*, a tumor suppressor gene for thymic lymphomas [23,25,26], because these deletions are frequently generated by aberrant V(D)J recombination during the thymocyte development [25]. Hence, if a thymocyte with the mutation preferentially proliferates in atrophic thymus following irradiation, the clonal growth should be detectable by examining *Bcl11b* intragenic deletions with nested PCR. DNA was extracted from thymus in mice at 28 days after irradiation and examined with nested PCR (Fig. 1B). The bands of *Bcl11b* intragenic deletions were detected in approximately a half of thymuses under these PCR condition (see Materials and methods). Although the intensities varied, the sizes of the bands were similar to that of the lymphoma DNA diluted 10^2- to 10^3-fold with brain DNA. Assuming that the thymus contained 3×10^7 cells, the number of thymocytes with *Bcl11b* mutations was estimated from the band intensities as approximately 10^5 in a thymus. The result indicates the presence of clones in some of thymuses at 28 days after irradiation, which suggests that the clonal growth of possible prelymphoma cells starts at a very early stage during the lymphoma development.

Detection of ROS in thymocytes in vivo

Radiation has been shown to increase ROS levels in *in vitro* irradiated cells and their progeny [14,15,27]. However, a few studies investigate the *in vivo* effect of IR on the ROS

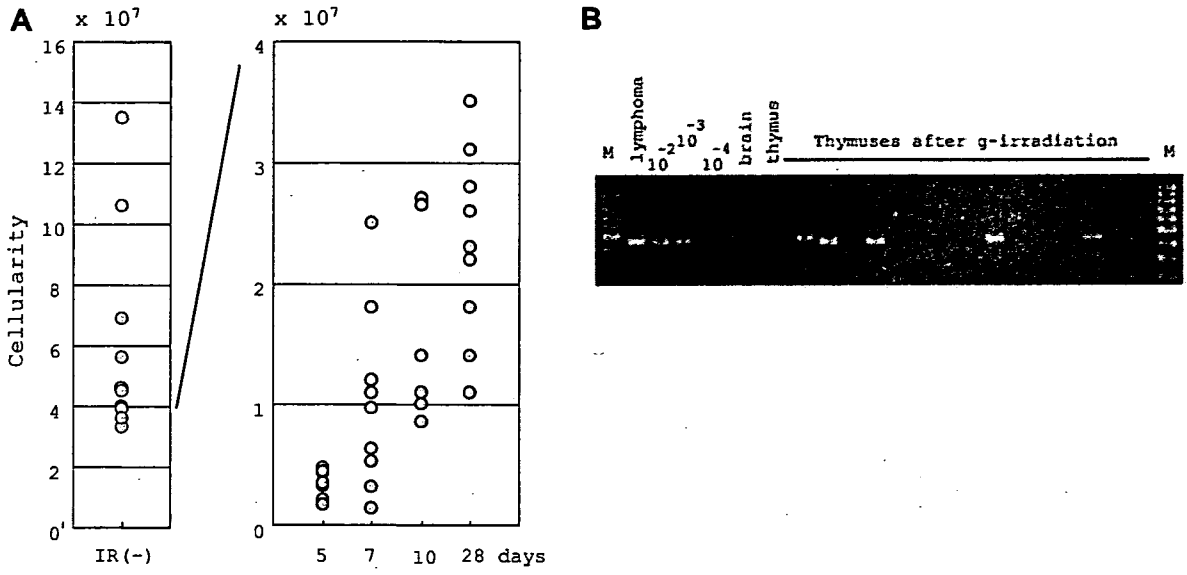

Fig. 1. (A) Cellularity of thymocytes at various times after 3 Gy γ-irradiation. (B) Existence of clonally growing thymocytes in thymuses at 28 days after irradiation. Nested PCR of *Bcl11b* intragenic deletions was performed and the PCR products were compared to the deletion-positive lymphoma DNA which had been 10^2-, 10^3-, and 10^4-fold diluted with brain DNA.

evels. We examined such effects on thymocytes that were solated from BALB/c mice at 5, 7, 10, and 28 days after he irradiation. Thymocytes were analyzed with flow ytometry after incubation with DCFH-DA, which is a nembrane-permeable fluorescent dye and the oxidization of DCFH-DA to DCF by ROS results in increased fluorescence of the dye.

Fig. 2A shows examples of the forward scatter and side catter analysis of unirradiated thymus and thymus at 7 lays after 3 Gy irradiation. The proportion of dead cells nd debris increased after irradiation. The dead cells and lebris-excluded fraction of thymocytes showed significant ncrease in DCF fluorescence after IR and the increase vas higher at 5 days than at 7 days after (upper panels in Fig. 2B). These results suggested an increase in ROS in thymocytes of irradiated mice. The ROS levels of thymocytes at 10 and 28 days after irradiation were similar to those of unirradiated thymocytes (data not shown). In parallel with he increase in ROS, however, the proportion of large cell-sized thymocytes increased in the irradiated samples (lower panels in Fig. 2B). Therefore, the ROS level was separately examined in the large cell-sized and small cell-sized fractions of thymocytes. The large thymocytes were found to have higher levels of ROS than the small thymocytes did Fig. 2C). Of note is that although the proportion of large hymocytes was very low, the level of ROS in the large thymocytes from unirradiated thymus was as high as that rom irradiated thymus. This indicated that the high ROS vas the feature of large thymocytes and not due to rradiation.

Properties of small and large thymocytes were investigated by flow-cytometric analysis of cell surface markers. A lower proportion of $CD4^+CD8^+$ double positive cells was found in large thymocytes than in small thymocytes, suggesting that large thymocytes comprised more immature cells than small thymocytes (Fig. 2D). This characteristic of large thymocytes was independent of irradiation status. However, irradiation increased the proportion of immature subsets of thymocytes ($CD4^-CD8^-$ and $CD4^-CD8^+$ cells) in both small and large thymocytes. We next examined BrdU uptake in thymocytes to test the capability for those small and large thymocytes to proliferate (Fig. 2E). Only large thymocytes incorporated BrdU, irrespective of irradiation (data not shown), indicating that the large cells comprise of cycling cells. A high ROS level has been shown to activate p53 tumor suppressor. Hence, the activation was examined by Western blotting. A higher expression of p53 was found in the large thymocytes relative to the small thymocytes (Fig. 2F). Taken together, these results suggest that irradiation increases the number of the immature large thymocytes with high ROS levels and a proliferation capacity. Since ROS can cause DNA damage, the large thymocytes are the likely target for precancerous conversion with clonal expansion.

Higher retention of large thymocytes in susceptible strain than resistant strain

Mtf-1 congenic heterozygous mice of BALB/c(C) background carrying an MSM(M)-derived 4 Mb interval (Fig. 3A) were mated with each other, and progeny were used for flow-cytometric analysis at 7 days after 3 Gy irradiation. We always used unirradiated thymocytes as a control, setting region gates for large thymocytes to range from 15% to 18%. Under the same gate condition, the proportion of large thymocytes was shown to range from 15%

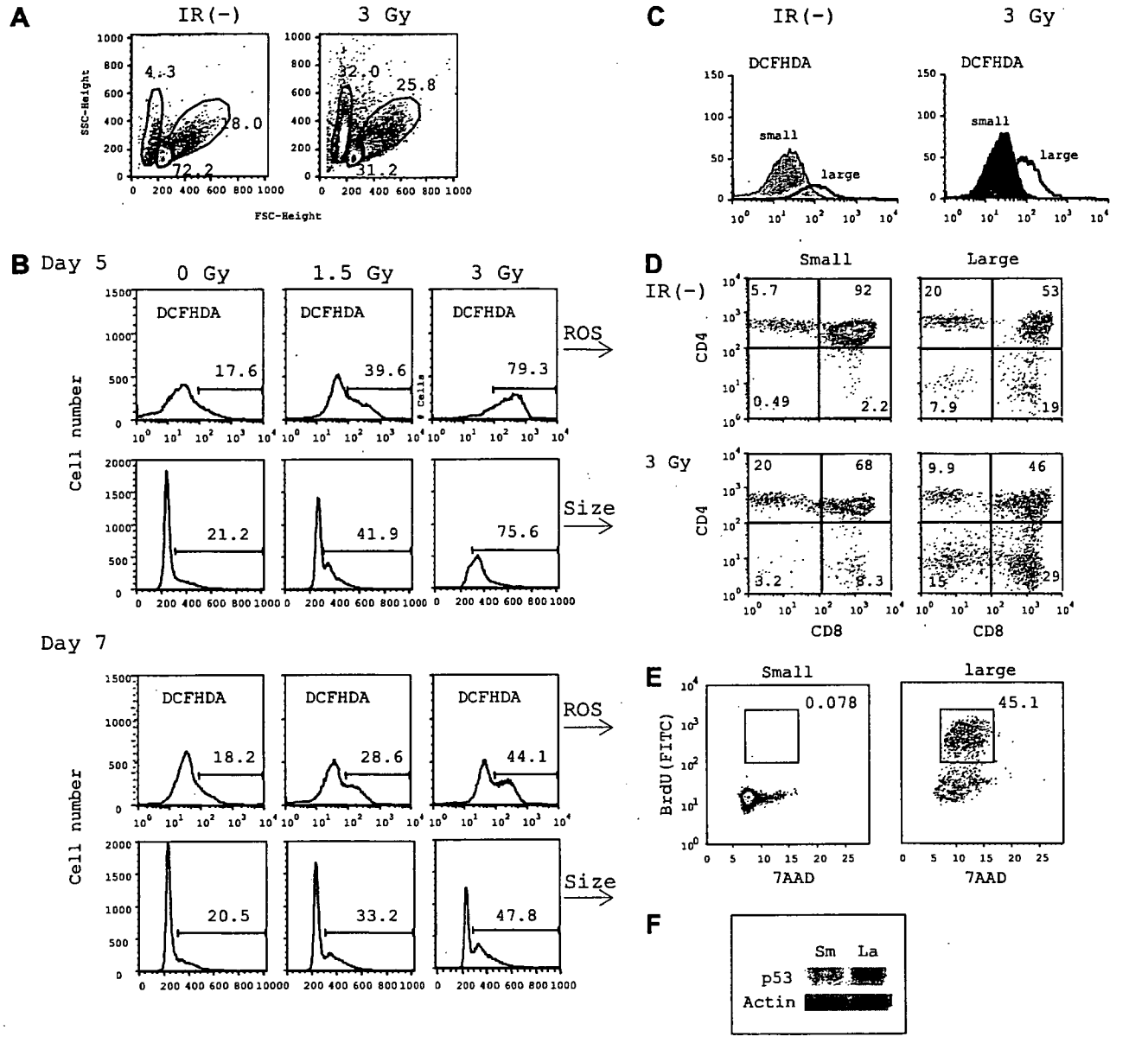

Fig. 2. IR increases the number of large thymocytes with high levels of ROS. (A) Cell size of thymocytes by forward scatter (FSC) versus side scatter (SSC) was analyzed by flow cytometry in unirradiated BALB/c mice and mice at 7 days after irradiation. The percentages of cells are shown in corresponding areas. (B) ROS levels (upper) and the cell size (lower) of thymocytes at 5 and 7 days after irradiation. The horizontal bars indicate percentages of cells in corresponding areas. (C) ROS levels of small and large thymocytes at 7 days after irradiation. (D) Surface expression of CD4 and CD8 on thymocytes was analyzed by flow cytometry in small and large thymocytes at 7 days after irradiation. (E) The measurement of cells incorporated BrdU and total DNA content in small and large thymocytes. The region gate in FACS analysis of large thymocytes indicated that 45.1% of the cells actively incorporated BrdU whereas that of small thymocytes showed that only 0.078% of the cells actively incorporated BrdU. (F) Western blotting indicated an increase of p53 in large thymocytes relative to small thymocytes.

to 60% in irradiated mice. Thymuses were analyzed for the proportion of large thymocytes in mice of the three different *Mtf-1* genotypes (Fig. 3B). We then divided thymuses into two groups, one harboring large thymocytes above the level of 20% and the other harboring large thymocytes below 20%. The former retains radiation influences and can be regarded as a high-risk group with clonally expanding precancerous cells. The latter, on the other hand, seems to be the thymuses well recovered from radiation influences.

Our previous results showed that mice of *Mtf-1* C/C and C/M genotypes are susceptible to γ-ray-induced thymic lymphomas and those of *Mtf-1* M/M genotype resistant [9,13]. A total of 18 mice of C/C and C/M genotype belonged to the former with more than 20% large thymocytes and only four belonged to the latter with less than

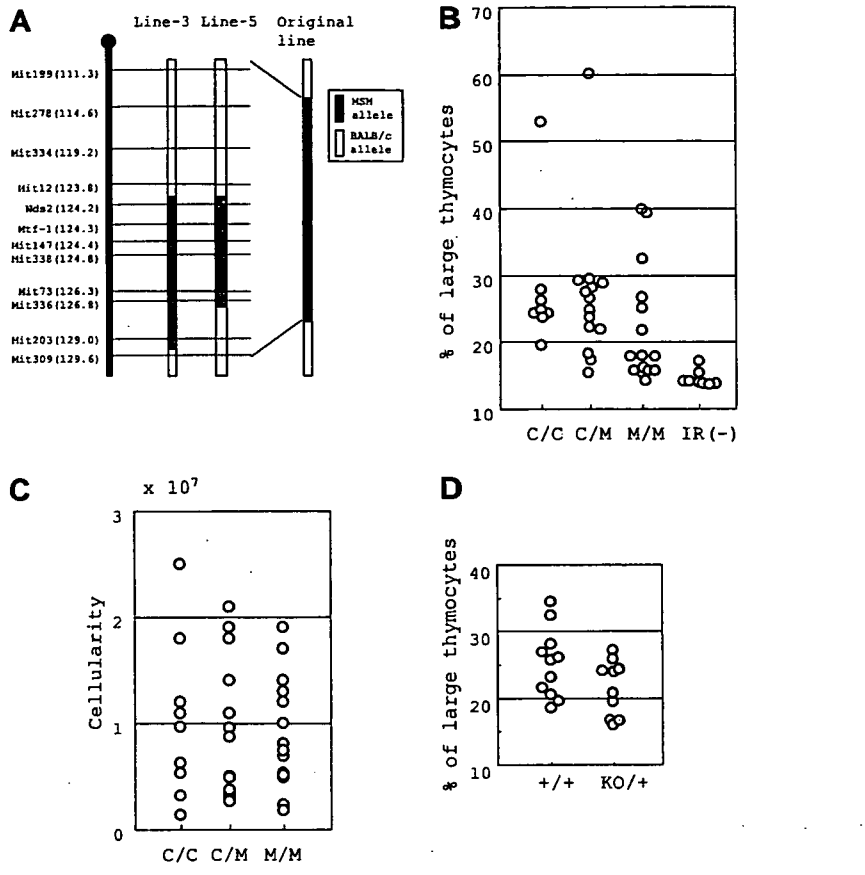

Fig. 3. Higher retention of large thymocytes in susceptible congenic mice. (A) Genetic constitution is displayed of congenic mouse strains (line-3 and line-5) of BALB/c background. The line-5 is a subcongenic line derived from the line-3 mice. Vertical bars represent a chromosomal region with map positions in Mb from the centromere) and shadowed portions carry an MSM-derived region. (B) Distribution of thymuses with different percents of large thymocytes was analyzed in mice of the three different *Mtf-1* genotypes: C/C, C/M, and M/M genotypes. (C) Cellularity of thymocytes was analyzed in mice of the C/M and M/M *Mtf-1* genotypes at 7 days after γ-irradiation. (D) Distributions of thymuses with different percents of large thymocytes were analyzed in mice of Bcl11b$^{+/+}$ and Bcl11b$^{KO/+}$.

20%. In contrast, six mice of M/M genotype were belonged to the former and nine to the latter. This difference between susceptible mice and resistant mice is statistically significant (χ^2 test, $P = 0.0089$), indicating the tendency of susceptible strains retaining large thymocytes more than the resistant strain. We noted that the four thymuses possessing more than 40% of large thymocytes were very atrophic (see the open circles in Fig. 3B). On the other hand, no significant difference in the cellularity was observed between mice of *Mtf-1* C/C and C/M genotypes and mice of M/M genotype (Fig. 3C). Analysis of thymocytes with different ROS levels showed a similar pattern of different distributions (data not shown).

Bcl11b-knockout heterozygous mice are more susceptible to γ-ray-induced thymic lymphomas than *Bcl11b* wild-type mice (Kamimura et al., accompanying paper). Thus, analyses of large thymocytes were carried out on *Bcl11b* wild-type and heterozygous mice (Fig. 3D). The proportion of large thymocytes ranged from 16% to 40% in irradiated mice and no significant difference was observed between *Bcl11b* wild-type and knockout heterozygous mice. These results suggest that *Mtf-1* susceptibility locus and *Bcl11b* tumor suppressor gene contribute to the development of radiogenic thymic lymphomas by distinct mechanisms.

Discussion

This paper examines clonal growth of thymocytes after irradiation, early effects of IR on cell behavior *in vivo* and its difference between *Mtf-1* susceptible and resistant congenic mice for γ-ray-induced thymic lymphomas, to reveal the basis for the increased susceptibility given by *Mtf-1* locus. Here, we show thymocytes clonally growing at 28 days after irradiation, indicating the start of clonal expansion at a very early stage. We also show that susceptible mice tended to have more of proliferating immature large thymocytes with higher ROS levels than resistant mice when examined at 7 days after irradiation. This increase of large thymocytes may be a compensatory reaction of thymocytes to depletion of the cells after irradiation. Of particular importance is that the mode of the

compensatory reaction differed between susceptible and resistant mice. The high proportion of the large thymocytes is likely to contribute to lymphoma susceptibility because they are vulnerable to ROS-induced mutation. The importance of the cell death and complementary proliferation for carcinogenesis is also provided by the study on hepatocellular carcinogenesis [28].

Genetic factors underlying cancer susceptibility are best treated as quantitative trait loci [29,30] and in most cases the susceptibility does not operate in the gain-or-loss mechanism which is for the oncogenes and tumor suppressor genes conferring cancerous phenotype of the cell [31,32]. An individual mouse with a predisposing genotype may not develop cancer, while mice with the predisposing genotype will on average exhibit a higher incidence of cancer over those without. Indeed, *Mtf-1* susceptible mice developed thymic lymphomas at the incidence of approximately 70% whereas resistant mice exhibited that of 40% [9,13]. Susceptibility genes may predispose by affecting the level of genomic insult to the cancer target cells (that is, the initiation frequency), the promotion of tumor cell proliferation and growth, and the number of the target cells. This study showed that the *Mtf-1* susceptible gene contributes to the persistence of large thymocytes after irradiation but not to the total number of thymocytes. These suggest that the *Mtf-1* susceptibility affects the number of the large thymocytes, the candidate target cells for malignant conversion. This may be supported by the fact that the *Mtf-1* susceptibility gave the higher incidence of thymic lymphomas but did not affect the latency [9,13]. In contrast, KO heterozygosity of the *p53* and *Bcl11b* genes gave both the higher incidence and the shorter latency probably due to the pre-existence of one hit of mutation ([33]; Kamimura et al., unpublished paper).

In the present study, differences were found in radioresponses of thymocytes in the congenic mice of BALB/c background carrying an MSM-derived 4 Mb region between *Nds2* and *D4Mit336*. Therefore, the difference can be ascribed to a gene or genes in this region and the *Mtf-1* gene in this interval is obviously a strong candidate for the susceptibility gene. At present, the mechanism of *Mtf-1* alleles for affecting the retention of large thymocytes is unclear. In addition, there are many genes within this interval other than *Mtf-1*. Therefore, the observed phenotypic difference may not solely be attributable to the *Mtf-1* polymorphism. The relationship between *Mtf-1* and the susceptibility remains to be further investigated.

Acknowledgments

We thank O. Niwa for critical reading of the manuscript. This work was supported by Grants-in-Aid of Second Term Comprehensive 10-year Strategy for Cancer Control from the Ministry of Health, Labor and Welfare of Japan.

References

[1] H.S. Kaplan, The role of radiation in experimental leukemogenesis, Natl. Cancer Inst. Monogr. 14 (1964) 207–217.
[2] F.C. Ludwig, R.M. Elashoff, J.S. Wellington, Murine radiation leukemia and the preleukemic state, Lab. Invest. 19 (1968) 240–251.
[3] R. Kominami, O. Niwa, Radiation carcinogenesis in mouse thymic lymphomas, Cancer Sci. 97 (2006) 575–581.
[4] T. Sado, H. Kamisaku, E. Kubo, Bone marrow–thymus interactions during thymic lymphomagenesis induced by fractionated radiation exposure in B10 mice: analysis using bone marrow transplantation between Thy 1 congenic mice, J. Radiat. Res. 32 (1991) 168–180.
[5] H.S. Kaplan, W.H. Carnes, M.B. Brown, B.B. Hirsch, Indirect induction of lymphomas in irradiated mice. I. Tumor incidence and morphology in mice bearing nonirradiated thymic grafts, Cancer Res. 16 (1956) 422–425.
[6] C. Humblet, M.P. Defresne, R. Greimers, A.M. Rongy, J. Boniver, Further studies on the mechanism of radiation induced thymic lymphoma prevention by bone marrow transplantation in C57BL mice, Leukemia 3 (1989) 813–818.
[7] M. Muto, E. Kubo, T. Sado, Development of prelymphoma cells committed to thymic lymphomas during radiation-induced thymic lymphomagenesis in B10 mice, Cancer Res. 47 (1987) 3469–3472.
[8] H. Kamisaku, S. Aizawa, M. Kitagawa, Y. Ikarashi, T. Sado, Limiting dilution analysis of T-cell progenitors in the bone marrow of thymic lymphoma-susceptible B10 and -resistant C3H mice after fractionated whole-body X-irradiation, Int. J. Radiat. Biol. 72 (1997) 191–199.
[9] Y. Saito, Y. Ochiai, Y. Kodama, et al., Genetic loci controlling susceptibility to gamma-ray-induced thymic lymphoma, Oncogene 20 (2001) 5243–5247.
[10] H. Sato, Y. Tamura, Y. Ochiai, Y. Kodama, K. Hatakeyama, O. Niwa, R. Kominami, The *D4Mit12* locus on mouse chromosome 4 provides susceptibility to both γ-ray induced and *N*-methyl-*N*-nitrosourea-induced thymic lymphomas, Cancer Sci. 94 (2003) 668–671.
[11] F. Radtke, O. Georgiev, H.P. Muller, E. Brugnera, W. Schaffner, Functional domains of the heavy metal-responsive transcription regulator MTF-1, Nucleic Acids Res. 23 (1995) 2277–2286.
[12] U. Wimmer, Y. Wang, O. Georgiev, W. Schaffner, Two major branches of anti-cadmium defense in the mouse: MTF-1/metallothioneins and glutathione, Nucleic Acids Res. 33 (2005) 5715–5727.
[13] Y. Tamura, M. Maruyama, Y. Mishima, H. Fujisawa, M. Obata, Y. Kodama, Y. Yoshikai, Y. Aoyagi, O. Niwa, W. Schaffner, R. Kominami, Predisposition to mouse thymic lymphomas in response to ionizing radiation depends on variant alleles encoding metal responsive transcription factor-1 (Mtf-1), Oncogene 24 (2005) 399–406.
[14] J.B. Little, Radiation carcinogenesis, Carcinogenesis 21 (2000) 397–404.
[15] J.L. Redpath, M. Gutierrez, Kinetics of induction of reactive oxygen species during the post-irradiation expression of neoplastic transformation in vitro, Int. J. Radiat. Biol. 77 (2001) 1081–1085.
[16] A.L. Jackson, L.A. Loeb, The contribution of endogenous sources of DNA damage to the multiple mutations in cancer, Mutat. Res. 477 (2001) 7–21.
[17] R.S. Balaban, S. Nemoto, T. Finkel, Mitochondria, oxidants, and aging, Cell 120 (2005) 483–495.
[18] N.S. Chandel, P.T. Schumacker, R.H. Arch, Reactive oxygen species are downstream products of TRAF-mediated signal transduction, J. Biol. Chem. 276 (2001) 42728–42736.
[19] S.H. Jo, C . Yang, Q. Miao, M. Marzec, M.A. Wasik, P. Lu, Y.L. Wang, Peroxisome proliferator-activated receptor gamma promotes lymphocyte survival through its actions on cellular metabolic activities, J. Immunol. 177 (2006) 3737–3745.
[20] T. Criswell, K. Leskov, S. Miyamoto, G. Luo, D.A. Boothman, Transcription factors activated in mammalian cells after clinically relevant doses of ionizing radiation, Oncogene 22 (2003) 5813–5827.

[21] A.A. Sablina, A.V. Budanov, G.V. Ilyinskaya, L.S. Agapova, J.E. Kravchenko, P.M. Chumakov, The antioxidant function of the p53 tumor suppressor, Nat. Med. 11 (2005) 1306–1313.
[22] P. Lichtlen, W. Schaffner, Putting its fingers on stressful situations: the heavy metal-regulatory transcription factor MTF-1, Bioessays 23 (2001) 1010–1017.
[23] Y. Wakabayashi, H. Watanabe, J. Inoue, N. Takeda, J. Sakata, Y. Mishima, J. Hitomi, T. Yamamoto, M. Utsuyama, O. Niwa, S. Aizawa, R. Kominami, *Bcl11b* is required for differentiation and survival of αβ T lymphocytes, Nat. Immunol. 4 (2003) 533–539.
[24] J. Inoue, T. Kanefuji, K. Okazuka, H. Watanabe, Y. Mishima, R. Kominami, Expression of TCRαβ partly rescues developmental arrest and apoptosis of αβT cells in Bcl11b$^{-/-}$ mice, J. Immunol. 176 (2006) 5871–5879.
[25] J. Sakata, J. Inoue, H. Ohi, H. Kosugi-Okano, Y. Mishima, K. Hatakeyama, O. Niwa, R. Kominami, Involvement of V(D)J recombinase in the generation of intragenic deletions in the Bcl11b/Bcl11b tumor suppressor gene in γ-ray-induced thymic lymphomas and in normal thymus of the mouse, Carcinogenesis 25 (2004) 1069–1075.
[26] Y. Wakabayashi, J. Inoue, Y. Takahashi, A. Matsuki, H. Kosugi-Okano, T. Shinbo, Y. Mishima, O. Niwa, R. Kominami, Homozygous deletions and point mutations of the *Rit1/Bcl11b* gene in γ-ray induced mouse thymic lymphomas, Biochem. Biophys. Res. Commun. 301 (2003) 598–603.
[27] R.E. Rugo, R.H. Schiestl, Increases in oxidative stress in the progeny of X-irradiated cells, Radiat. Res. 162 (2004) 416–425.
[28] S. Maeda, H. Kamata, J.L. Luo, H. Leffert, M. Karin, IKKbeta couples hepatocyte death to cytokine-driven compensatory proliferation that promotes chemical hepatocarcinogenesis, Cell 121 (2005) 977–990.
[29] B.A. Ponder, Cancer genetics, Nature 411 (2001) 336–341.
[30] A. Balmain, Cancer as a complex genetic trait: tumor susceptibility in humans and mouse models, Cell 108 (2002) 145–152.
[31] D. Hanahan, R.A. Weinberg, The hallmarks of cancer, Cell 100 (2000) 57–70.
[32] C.J. Sherr, Principles of tumor suppression, Cell 116 (2004) 235–246.
[33] C.J. Kemp, T. Wheldon, A. Balmain, p53-deficient mice are extremely susceptible to radiation-induced tumorigenesis, Nat. Genet. 8 (1994) 66–69.

Dig Dis Sci (2007) 52:995–1000
DOI 10.1007/s10620-006-9278-y

Collagenous Gastritis: Endoscopic and Pathologic Evaluation of the Nodularity of Gastric Mucosa

Kenya Kamimura · Masaaki Kobayashi · Rintaro Narisawa · Hidenobu Watanabe · Yuichi Sato · Terasu Honma · Atsuo Sekine · Yutaka Aoyagi

Received: 15 November 2005 / Accepted: 1 March 2006 / Published online: 7 March 2007

Keywords Collagenous gastritis · Endoscopic ultrasonography · Collagen band · Mucosal nodularity

Introduction

Collagenous gastritis is a rare disorder, with 20 cases reported in the English literature to date [1–15]; the pathogenesis and prognosis remain unknown. Collagenous gastritis is defined histologically by the presence of a subepithelial collagen band thicker than 10 μm in association with increased inflammatory cell infiltrate of the lamina propria [9] and it is therefore straightforward to make a histological diagnosis from a biopsy specimen. While mucosal nodularity of the stomach is a characteristic finding, observed in 8 [1, 6, 7, 12–15] of the previous 20 cases, the endoscopic findings of collagenous gastritis have not been fully examined and no reports have investigated the findings of endoscopic ultrasonography (EUS) and the morphogenesis of this nodularity endoscopically and histologically. Furthermore, no report has discriminated endoscopically the mucosal nodularity in collagenous gastritis from a similar appearance in other diseases. In this article, focusing on these points, we report an additional case of collagenous gastritis with mucosal nodularity.

K. Kamimura (✉) · M. Kobayashi · Y. Sato · T. Honma · Y. Aoyagi
Division of Gastroenterology and Hepatology, Graduate School of Medical and Dental Sciences, Niigata University, Asahimachi 1-757, Niigata 951-8122, Japan
e-mail: kenya-k@med.niigata-u.ac.jp

R. Narisawa
Department of Endoscopy, Niigata University Medical and Dental Hospital, Niigata, Japan

H. Watanabe
Division of Molecular and Diagnostic Pathology, Graduate School of Medical and Dental Sciences, Niigata University, Niigata, Japan

A. Sekine
Internal Medicine, Niigata Prefectural Yoshida Hospital, Niigata, Japan

Case report

A 35-year-old Japanese man without gastrointestinal symptoms underwent upper gastrointestinal barium radiography for screening. As an abnormal surface with a mosaic-like pattern was observed in the body of the stomach (Fig. 1), the patient was referred to Niigata University Hospital, Niigata, Japan. There was no history of allergic disease, food allergy, or anti-inflammatory drugs. He had a history of epigastric pain 14 years previously and was diagnosed with gastritis by endoscopic examination at Yoshida Hospital. The symptoms improved immediately, and after the episode, the patient had no epigastric discomfort and received no medical treatment. The physical examination and laboratory data were normal including serum gastrin, pepsinogen I, pepsinogen II, and pepsinogen I(II ratio. Anti-*Helicobacter pylori* IgG and a urease breath test were also negative.

Endoscopic findings

Upper gastrointestinal endoscopy showed diffuse nodularity of the gastric mucosa in the antrum (Fig. 2) and in the greater curvature of the gastric body (Fig. 3A). Normal-looking mucosa was seen in the greater curvature of the lower body

Fig. 1 Double-contrast radiography demonstrates an abnormal surface with a mosaic-like pattern in the body of the stomach

between the nodular lesion in the antrum and the lesion in the gastric body. There were no gastric hemorrhages or ulcerative lesions. The chromoendoscopy revealed that the nodularity was composed of mucosal nodules 1–5 mm in diameter. The mucosa between the nodules was discolored and relatively depressed but did not cause erosive change (Fig. 3B). Mucosal nodularity spread widely to all of the greater curvature of the gastric body and its appearance became unclear by filling the stomach with sufficient air.

We reviewed the endoscopic pictures of 14 years previously and they suggested that there was already mucosal nodularity in the gastric body at that time (Fig. 4), although nodularity was not recognized in the antrum. The nodular appearance had become prominent in the antrum over a 14-year period and was supplemented in the body.

A 20-MHz EUS radial scanning probe (GFUM-Q240; Olympus, Tokyo) yielded cross-sectional images of the mucosa and submucosa. EUS for the nodular lesions of the greater curvature of the middle body revealed that the thickness of the second hypoechoic mucosal was variable and uneven, while the third hyperechoic submucosal layer was uniformly preserved (Fig. 5). The EUS did not show a subepithelial collagen band. These findings suggest that nodularity results from the irregular thickness of mucosal layer, and not

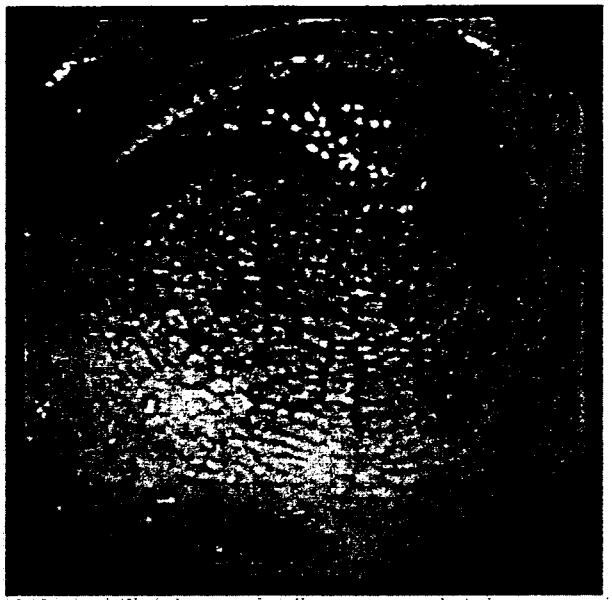

Fig. 2 Endoscopic view with indigo carmine staining, showing a regular nodular pattern in the antrum of the stomach

from the change of the submucosal layer. There were no abnormalities in the esophagus, duodenum, terminal ileum, or colorectum on endoscopy or in the small intestine on the barium radiograph.

Pathology

Biopsy specimens were obtained from 14 points along the entire gastric mucosa. The specimen from a nodule in the greater curvature of the body showed lamina propria lymphoplasmacytosis and a thickened subepithelial collagen band of less than 10 μm with no remarkable inflammation. The mucosa was not thickened and the glandular structure was well preserved in the nodule (Fig. 6). The mucosa near the nodule showed a thick, 50- to 100-μm collagen band and prominent infiltration of inflammatory cells, such as lymphocytes and eosinophils. In the lamina propria, inflammatory infiltrates were remarkable and destructive to glands, resulting in mucosal thinning. Collagen band mucosa was always associated with increased inflammatory cells. The collagen plate contained many entrapped superficial capillaries and inflammatory cells. Focal surface epithelial damage was present, such as epithelial cell flattening and partial detachment of the epithelium (Fig. 7). These findings tended to vary and were irregular even within biopsy specimens. The collagen band was also confirmed histochemically by Masson trichrome staining (data not shown). According to the updated Sydney system for the classification of gastritis [16], there were moderate chronic interstitial inflammation and mild neutrophil polymorph activity. Mild atrophy was seen with a type of pseudopyloric gland. *Helicobacter*

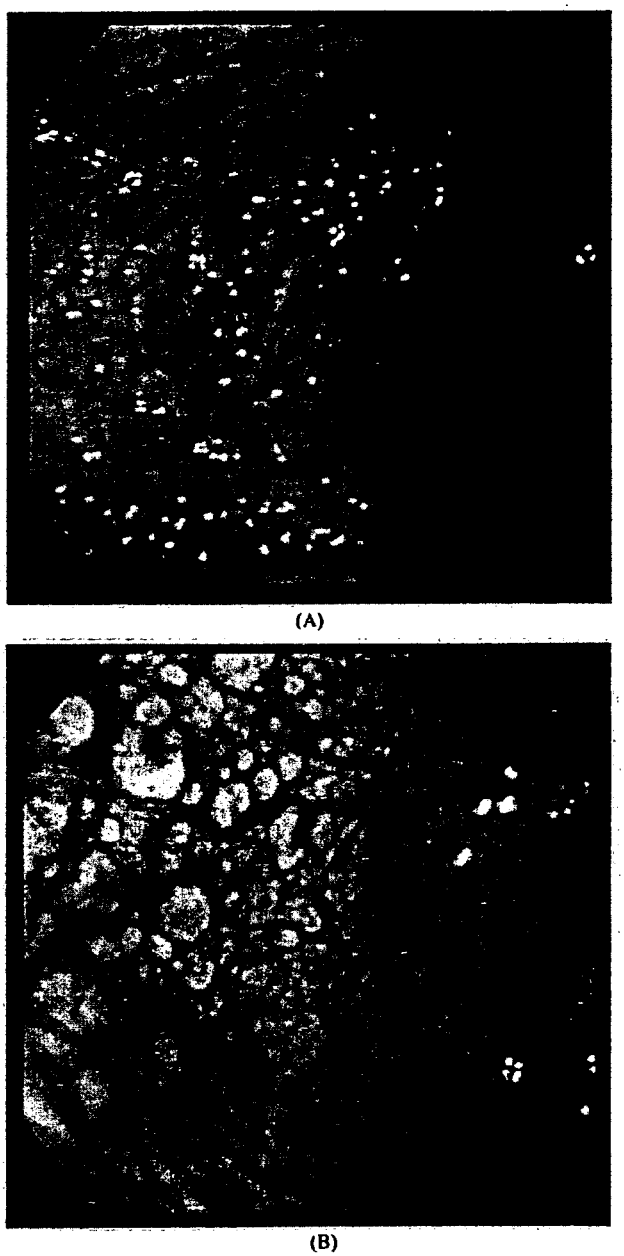

Fig. 3 Endoscopic view of the greater curvature of the gastric body. (A) Diffuse nodularity of the mucosa is present. (B) The nodular lesion is a group of nodules 1–5 mm in diameter

pylori was absent. Mild chronic inflammation was observed in biopsy specimens from the lesser curvature which did not show nodules. Biopsies from the duodenum, colorectum, and terminal ileum were normal, with no collagenous deposit.

A specimen obtained from the mucosal nodularity of the gastric body 14 years previously showed a subepithelial collagen band averaging 20 μm with thick and mild inflammation (Fig. 8).

Fig. 4 Endoscopic view of the body of the stomach from the examination 14 years previously, showing less prominent nodularity

Discussion

We report a case of collagenous gastritis presenting with mucosal nodularity. Collagenous gastritis is an extremely rare clinicopathological entity, with 20 cases reported in the English literature to date from the United States, Germany, Canada, France, Spain, India, Japan, and Korea [1–15].

Endoscopically, mucosal nodularity is one of the characteristic findings of collagenous gastritis. A similar nodular appearance is observed in superficial-type malignant lymphoma of the stomach, showing local gastric areas swollen due to the mucosal involvement of lymphoma cells. These uniform nodules with irregular grooves or erosions have some resemblance to cobblestones; however, in collagenous gastritis, mucosal nodules are more irregular in size and

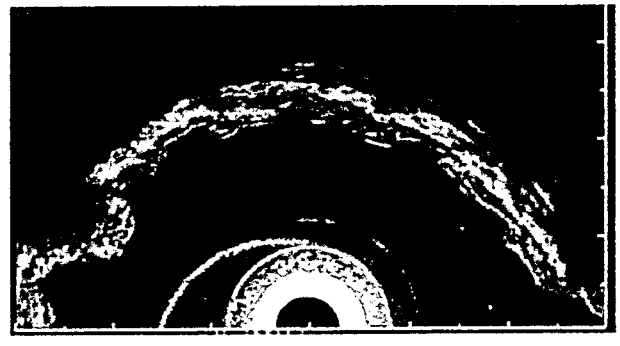

Fig. 5 Endoscopic ultrasonography images in the greater curvature of the gastric body with a nodular appearance. There was uneven thickening of the second hypoechoic layer